

UNIVERSITÄT REGENSBURG

Naturwissenschaftliche Fakultät II - Physik
Institut II - Experimentelle und Angewandte Physik



Blinking Phenomena in InGaN Quantum
Wells

Diplomarbeit von Christian Feldmeier aus Wörth a.d. Donau
unter Anleitung von PD Dr. Ulrich T. Schwarz von der Universität Regensburg
und Prof. Dr. Ruggero Micheletto von der Yokohama City University
durchgeführt an der Yokohama City University, Japan
Regensburg, November 2009

Contents

Introduction	1
I Background	3
1 InGaN/GaN quantum wells	5
1.1 Material system	5
1.2 Crystal structure	6
1.3 Internal electric fields	7
1.4 Spatial inhomogeneous indium distribution	7
1.5 GaN based LEDs	8
2 Random telegraph signal	11
2.1 Quantum jump theory	11
2.2 Power law	13
2.3 Deep traps and the random telegraph signal	14
3 Plasmons and coupling of quantum wells to plasmons	17
3.1 Bulk plasmons	17
3.2 Surface plasmons	18
3.2.1 Surface plasmon polaritons	18
3.2.2 Localized surface plasmons	19
3.3 Coupling of InGaN quantum wells to surface plasmons	21
3.4 Coupling of surface plasmons to light	23
3.5 Quantum confined stark effect screening vs. surface plasmon coupling	24
3.6 Plasmons in nanoclusters of metallic indium	25
II Experiments	27
4 Samples	29
5 Time intensity profiles	31
5.1 Method	31
5.2 Different types of blinking points	33

Contents

5.2.1	Two level blinking points	34
5.2.2	Multi level blinking points	35
5.2.3	Interpretation	38
6	Simulations	41
7	Temperature dependence of the blinking	45
7.1	Method	45
7.2	Photoluminescence changes	46
7.3	Two level blinking points	46
7.4	Multi level blinking points	46
8	Surface plasmons and the blinking phenomena	55
8.1	Photoluminescence enhancement	55
8.2	Changing emission pattern	56
8.3	SEM images	57
8.4	Cleaning the sample	60
8.5	Photoluminescence changes	60
8.6	Statistics on the changes	64
8.7	Comparisons between photoluminescence movies and SEM images	65
8.8	Changes in vacuum	67
9	Memory effect	73
9.1	Method	73
9.2	Photoluminescence changes	74
9.3	Systematic illumination interval sequence	76
	Summary	79
	Bibliography	81

Introduction

In the last decades the group III nitrides aluminum nitride (AlN), indium nitride (InN), gallium nitride (GaN) and their ternary alloys have gained much attention as a promising material system for a variety of semiconductor devices such as blue-emitting lasers, high-power transistors or bright light-emitting diodes (LED). GaN based LEDs are an interesting issue due to their role in full color display and lighting applications. Despite this importance the precise nature of the light emitting process hasn't been understood completely yet, due to the complex material physics and engineering involved [1,2].

An astonishing phenomenon that hasn't been understood yet is a blinking occurring in indium gallium nitride/gallium nitride (InGaN/GaN) quantum wells. At high indium content the photoluminescence of these quantum wells shows intense light emitting centers. Surprisingly some of these centers are optically not stable, their photoluminescence changes, they blink (fig. 0.1) [3].

An effect like this has been observed in a wide variety of scientific fields ranging from fluorescent proteins over polymers to semiconductor nanostructures. The link between these different areas is the unstable luminescence occurring always in nanoscale light emitters. As the blinking occurs in many different fields and systems, one might think there should be an universal answer to explain this nanoscale blinking, but even over ten years after the first observations a satisfactory explanation is without reach [4].

This thesis deals with the blinking phenomena in InGaN/GaN single quantum wells and should contribute to the understanding of the underlying mechanism. For this purpose a set of different experimental methods was applied to investigate on the blinking phenomenon. The thesis is structured as follows:

The first part introduces to the fundamental concepts that are of importance for studying the blinking phenomena in InGaN quantum wells. In chapter 1, properties of group III nitrides and InGaN quantum wells, special optical properties related to the experiments and the function of GaN based LEDs are explained. In chapter 2, different theoretical models describing a blinking behavior and associated causes are discussed. Chapter 3 concentrates on plasmons and the coupling of quantum wells to surface plasmons in metal surfaces, enabling them to enhance the emission of the quantum well. The coupling between InGaN quantum wells and surface plasmons in gold nanoparticles and gold films is especially addressed. In the second part of the thesis the materials, methods and experimental results of this work are discussed. The samples used for the experiments and their photo-

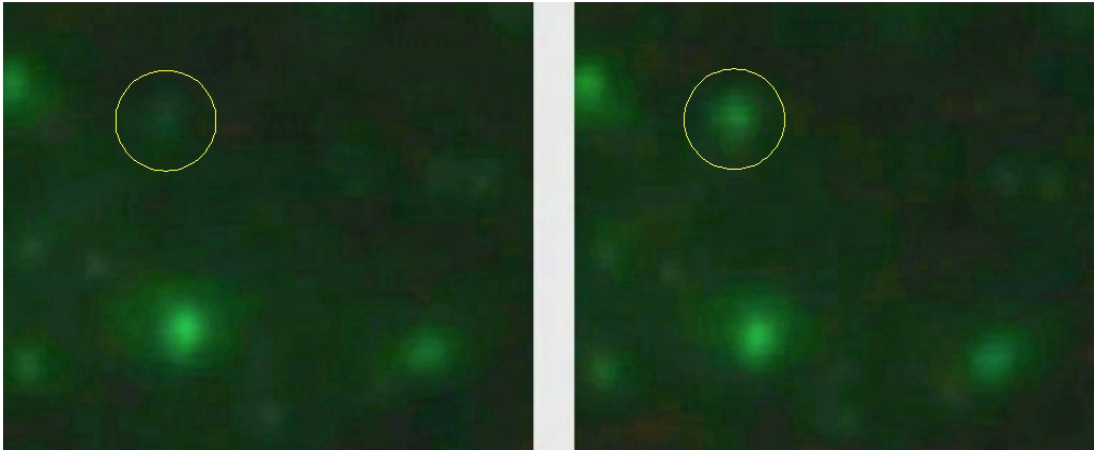


Figure 0.1: The images show the photoluminescence of a InGaN/GaN single quantum well at different times. Bright points of high intensity can be observed. The circled point changes intensity, it blinks. The size of the images is about $5 \times 5 \mu m$.

luminescent characteristics are described in chapter 4. In chapter 5, time intensity profiles of different blinking points are analyzed. The blinking is categorized into 3 different types of blinking by the number of intensity levels and different statistics involved. In this regard numerical simulations based on a theoretical model were done in chapter 6. After studying the dependence of the blinking behavior and statistics on the temperature in chapter 7, in chapter 8 surface plasmons coupling to InGaN quantum wells are addressed. New blinking points could be generated by means of enhanced light emission through surface plasmon coupling. In chapter 9, an optical memory effect of InGaN quantum wells was found by using a systematic illumination interval sequence. In the end the final part gives a brief summary of the obtained results.

Part I

Background

1 InGaN/GaN quantum wells

GaN based quantum heterostructures are the essential part of many important electrooptical devices such as light-emitting diodes (LEDs) or laser diodes. As all experiments of this thesis deal with optical effects in InGaN/GaN single quantum wells, this chapter will give a brief introduction to the properties of this remarkable materials and to effects related to the experiments.

1.1 Material system

The binary group III/group V direct bandgap semiconductor gallium nitride (GaN) and its ternary alloy with indium nitride (InN), indium gallium nitride (InGaN) provide the basis for InGaN quantum wells. For these structures a thin InGaN layer forming the active layer of the heterostructure is sandwiched between two thicker GaN layers. The smaller bandgap of InGaN results in a quantum well which is called single quantum well for one single layer of InGaN and multi quantum well for several layers of InGaN between layers of GaN.

The bandgap of InN $E_{g,InN}$ is about 0.7 eV lying in the infrared range and the one of GaN $E_{g,GaN}$ is about 3.4 eV lying in the ultraviolet range. Therefore in principle the bandgap of InGaN can range from ultraviolet to infrared, depending on the ratio of GaN to InN. The resulting band gap of InGaN $E_{g,InGaN}$ can be calculated by [5]:

$$E_{g,InGaN}(x) = xE_{g,InN} + (1 - x)E_{g,GaN} - bx(1 - x) \quad (1.1)$$

In this formula b is the bowing parameter which is 1.21 for the system InGaN, x describes the amount of InN, $(1 - x)$ accordingly the amount of GaN.

However, shifting the emission towards longer wavelengths demands higher concentrations of indium which results in lower efficiency. Additionally, technical problems in the growing of GaN with high indium contents limit the application of GaN based quantum wells to the range from near UV to green.

1 InGaN/GaN quantum wells

	InN	GaN
band gap E_g [eV]	0.7	3.4
lattice constant a [\AA]	3,545	3,189
lattice constant c [\AA]	5,703	5,185

Table 1.1: The lattice constants a and c and the band gaps E_g of indium nitride (InN) and gallium nitride (GaN)

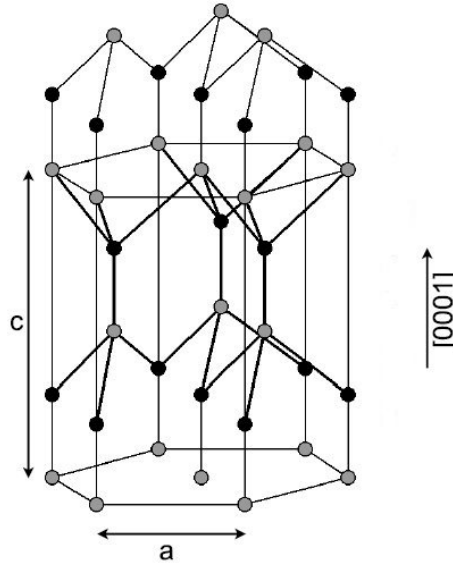


Figure 1.1: The hexagonal wurtzite structure of GaN or InN grown in $[0001]$ direction. Nitrogen atoms are black, gallium or indium ones are grey. (from [6])

1.2 Crystal structure

Group III nitrides can crystallize both in zinc blende and hexagonal wurtzite structure. As the wurtzite structure is thermodynamically much more stable it is usually used for electrooptical devices. Fig. 1.1 shows the wurtzite structure. It is a hexagonal crystal system with its unit cell characterized by the lattice parameters a, c and u. c is the distance between two identical hexagonal lattice planes, a the distance between the atoms in one lattice plane, u describes the bond length in c direction and thus the distortion of the unit cell. All group III nitrides GaN, InN and AlN and their ternary and quaternary compounds can have this crystal structure but with different lattice parameters a and c and different band gaps E_g . Table 1.1 shows a comparison of the lattice parameters and band gaps of InN and GaN.

Wurtzite structure lacks inversion symmetry i.e. the centres of positive and

negative charges are not identical. This and the fact that the III-N bond has strong ionic character leads to spontaneous polarization aligned along the [0001] direction. The lack of inversion symmetry gives also rise to special properties that are due to polarization such as piezoelectricity.

1.3 Internal electric fields

Internal electric fields play a very important role and have a strong impact on the properties of GaN based quantum wells. Apart from the spontaneous polarization strong piezoelectric fields occur. Caused by the different lattice constants of GaN and InN the thin InGaN film is strained in the quantum well i.e. its lattice parameters are not the same as the ones in equilibrium. This causes a strong piezoelectric field which can get as strong as 3 MV/cm for a Indium concentration of 22%. Compared to this the spontaneous polarization is very small (about 100 kV/cm) and neglectable [7].

The internal fields cause a deformation of the quantum well bands as shown in fig. 1.2. This results in a red shift of the emission towards longer wavelengths. As this is similar to the Stark effect in atom physics this effect is called quantum-confined Stark effect (QCSE). Along with this the internal fields cause a confinement of the electron and hole wavefunction on opposite sides of the quantum well separating the holes and electrons. The overlap between the electron (Ψ_e) and the hole wavefunction (Ψ_h) gets smaller compared to the situation without electrical field. This leads to a smaller oscillator strength which is the overlap integral of both functions. With decreasing oscillator strength the transition probability and thus the radiative combination efficiency decreases. In a wide quantum well (thick InGaN layer) this effects gets even more important because the separation of the wavefunctions is bigger.

Another electrical field inside the quantum well that has a strong influence on the optical properties is the electrical field arising from the separation of opposite charged carriers. The field between electrons and holes has the opposite direction of the piezoelectric field and therefore screens the piezoelectric field. The emission therefore shifts back to higher energies [8].

In LED structures there is an additional internal electrical field of the p-n junction which is directed from the p-doped to the n-doped area.

1.4 Spatial inhomogeneous indium distribution

The indium concentration is not homogeneously distributed in the InGaN layer. During the growing process InGaN tends to precipitate cluster like structures with especially high indium content. These clusters can clearly be observed in

1 InGaN/GaN quantum wells

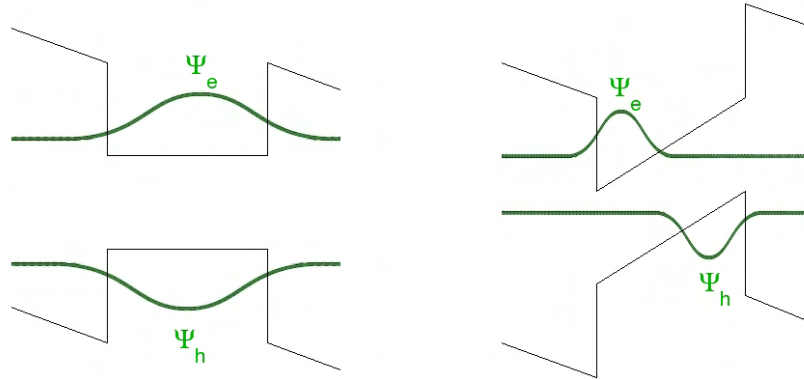


Figure 1.2: Scheme of the quantum confined stark effect (QCSE) (after [9]). The internal fields cause a deformation of the quantum well bands. This results in a red shift of the emission towards longer wavelengths. The electrons and the holes get confined on opposite sides of the quantum well leading to a separation of holes and electrons. The overlap between the electron (Ψ_e) and the hole wavefunction (Ψ_h) gets smaller. The transition probability and thus the radiative combination efficiency decreases, the quantum well emission gets weaker.

TEM images of the quantum well as reported in [10] and [11]. Spatially resolved photoluminescence showed that the spatial distributions of the optical properties of InGaN depend on the indium composition. Areas of high photoluminescence intensity coincide with areas of high indium content [12]. The band gap of areas of high indium content is smaller than the one of the surroundings with lower indium concentration. Carriers can be trapped and localized in these potential minima hindering the pathways to nonradiative recombination centres and thus increasing the probability for radiant recombination [13]. The sizes of the island like areas with high indium content can range from 20 nm to 70 nm [13], or just measure a few nanometers [14]. Other groups report on sizes as large as 0,2 to 1 μm [12].

1.5 GaN based LEDs

Quantum wells can be excited in several ways. The light emission is then referred to as photoluminescence, for excitation by means of electromagnetic radiation, as cathodoluminescence, when excited by a beam of electrons, as radioluminescence for ionizing radiation and as electroluminescence in the case of an exciting electric field.

Conventional light sources like light bulbs or fluorescent lamps work on the basis of either incandescence or discharge in gases. By contrast the light generation through LEDs is based on a fundamentally different process providing lots of advantages over conventional light sources. LEDs are characterized by their small

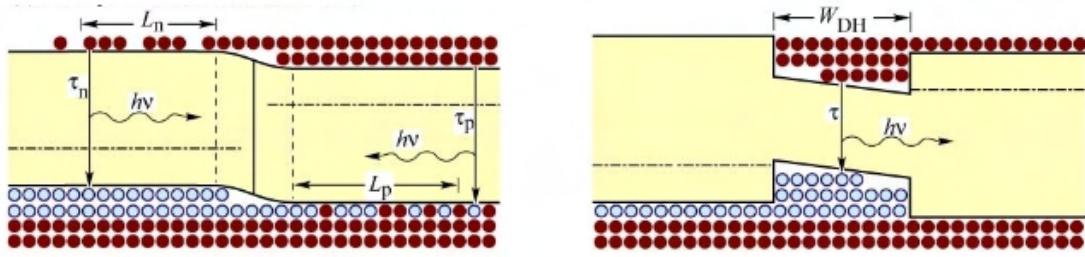


Figure 1.3: The schematic diagram shows a p-n homojunction (left) and a p-n heterojunction (right) both under forward bias. In homojunctions, carriers diffuse over the diffusion lengths L_n and L_p before they recombine. In heterojunctions, carriers are confined by the quantum well. (adapted from [16])

size and weight, better efficiency permitting energy savings, long lifetime and durability and control over emission properties.

LEDs consist of a p- and a n-doped semiconductor layer. Donor impurities create states near the conduction band while acceptors create states near the valence band. This shifts the Fermi level closer to the conduction bands for n-doped semiconductors and closer to the valence band in the case of p-doped semiconductors. Joining these different doped semiconductors together in very close contact results in a p-n junction. Electrons diffuse into the p-doped area whereas holes diffuse into the n-doped area causing a space charge in the so called depletion layer. The electric field of the space charge opposes the diffusion process in equilibrium state. Applying forward bias removes this equilibrium state and injects electrons from the n-side into the p-n junction where they recombine with holes (fig. 1.3).

During the recombination radiative recombination processes compete with non-radiative processes. To obtain high efficiencies as many electron-hole couples as possible have to recombine radiating photons. This means the non-radiative carrier lifetime τ_{nr} should be large compared to the radiative carrier lifetime τ_r . With this the quantum efficiency η can be defined as [17]:

$$\eta = \frac{\tau_{nr}}{\tau_{nr} + \tau_r} \quad (1.2)$$

expressing the ratio of exited carriers that relax via radiative recombination to the total recombination.

Often a thin semiconducting layer with smaller bandgap than the surrounding areas is located between the p- and the n-doped area. The resulting quantum well confines both the electrons and the holes resulting in higher recombination probability and increasing efficiency (fig. 1.3). The emission wavelength hence depends on the quantum well band gap and the width of the quantum well influencing on the strength of the quantum confined Stark effect. Due to their bandstructure InGaN/GaN quantum wells are used for LEDs emitting in the

1 InGaN/GaN quantum wells

range from UV to green [16, 17].

2 Random telegraph signal

The blinking points observed for this thesis show different blinking behaviors (section 5.2). We think that all these different kinds of blinking are based on one fundamental blinking behavior which randomly switches between just two intensity levels. A signal that switches between an on- and a off-state is called random telegraph signal (fig. 2.1). Such a signal has been observed in many different systems like macroscopic InGaN clusters [18] quantum dots [19,20] or, like in our case, in InGaN/GaN single quantum wells [3].

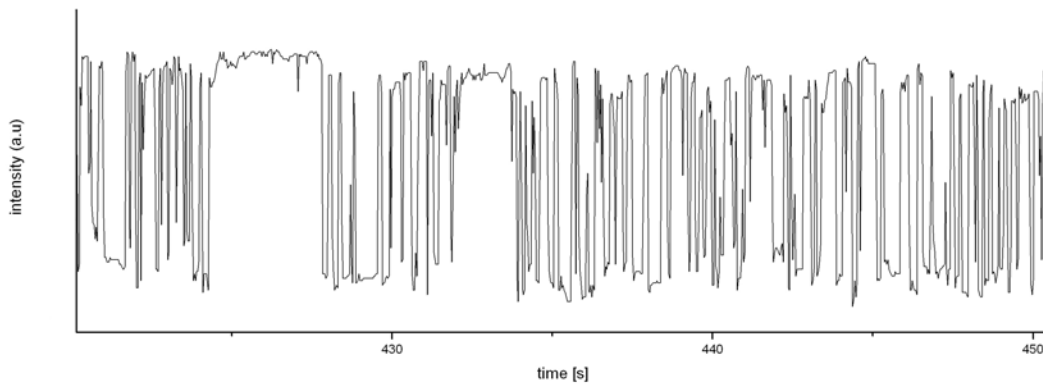


Figure 2.1: A time intensity profile of a blinking point that had been taken for this thesis. The blinking point shows random telegraph behavior. The intensity switches randomly between two levels, an on- and an off-state.

This section will give a brief introduction to different mechanisms that can cause a random telegraph signal and the different statistics and causes associated with them.

2.1 Quantum jump theory

The simplest model for the random telegraph signal was developed by Cook and Kimble [21]. It describes a fast fluorescent cycling of a electron between two states $|1\rangle$ and $|2\rangle$, interrupted by infrequent jumps to a third state $|3\rangle$, a metastable unfluorescent shelf state. From this third state the electron can relax into the

2 Random telegraph signal

ground state $|1\rangle$ and fluorescent cycling between the $|1\rangle$ and $|2\rangle$ starts again. The system is in the on state when the electron is cycling between $|1\rangle$ and $|2\rangle$ and in the off state when the electron is 'trapped' in state $|3\rangle$.

A quantum jump random telegraph signal like this has been observed in single ions or molecules [22, 23]. But also random telegraph signal of quantum dots that can be described by the quantum jump model could be found [19, 24]. Aoki *et al* [18] reported on random telegraph noise in the luminescence of individual macroscopic InGaN clusters. These clusters had been formed in InGaN multiple quantum wells and showed a blinking behavior with exponentially distributed probabilities of on and off times.

In the theory of Cook and Kimble [21] the intensity of the on state is considered to be $I_{on} = I_0$, the intensity of the off state is zero $I_{off} = 0$. The probability density for the off times T_{off} in the fluorescent signal is derived as:

$$W_{off}(T) = R_- e^{-R_- T} \quad (2.1)$$

And analogically the probability density for the on times:

$$W_{on}(T) = R_+ e^{-R_+ T} \quad (2.2)$$

R_+ is the transition rate from on- to off-state and R_- the transition rate from off- to on-state. Both distributions are exponential just varying in the different time constants R_+ and R_- .

Using the correlation function the frequency spectrum of the intensity fluctuations can be calculated to:

$$S(\omega) = \pi m_I^2 \delta(\omega) + \frac{\sigma_I^2 (R_+ + R_-)}{\omega^2 + (R_+ + R_-)^2} \quad (2.3)$$

with the mean intensity

$$m_I = \langle I \rangle = \frac{I_0 R_-}{R_+ + R_-} \quad (2.4)$$

and the variance of the intensity:

$$\sigma^2 = \langle I^2 \rangle - \langle I \rangle^2 = \frac{I_0^2 R_+ R_-}{(R_+ + R_-)^2} \quad (2.5)$$

Except for the first part, which is the zero-frequency component, the frequency spectrum is a Lorentzian.

This model is based on a single electron in the three level system. In the InGaN single quantum wells used for this thesis a large number of carriers are involved in the radiation process, which makes the situation somewhat different from this theory. Additionally the intensity in the off state of the blinking points in the InGaN single quantum wells is not zero as it would be in the quantum jump theory. Nevertheless this model can be applied to our system when the switching is attributed to a charging and discharging of a single localized state by a single carrier. This will be discussed in more detail in section 2.3.

2.2 Power law

Other groups reported on a random telegraphic blinking that didn't show exponential distribution of on and off times as predicted by the quantum jump theory. For example the blinking of single fluorescing nanocrystals of cadmium selenite showed power law statistics of on and off times [25,26] which indicate a much more complex underlying system than the quantum jump one.

The power law describes the relationship between two quantities, the size of an event and its probability. The sizes of power outages, the intensities of earthquakes or the population of cities are typical examples for power law distributions. Such distributions are signs for highly complex underlying processes. Mathematically a quantity x obeys the power law if the probabilities are distributed like

$$P(x) \propto x^{-\alpha} \quad (2.6)$$

The exponent α is called the scaling parameter and typically lies between $2 < \alpha < 3$ with some exceptions [27].

The most important property of a power law distribution is its scale invariance, i.e. a constant scaling factor c only causes a proportional scaling of the whole distribution:

$$P(cx) \propto P(x) \quad (2.7)$$

The integral

$$\int_0^{\infty} P(x)dx = \infty \quad (2.8)$$

diverges and therefore makes it impossible to identify an inherent scale of a problem that is described by a power law [4].

Blinking statistics following the power law have been attributed to a number of different causes. One model derives a potential law distribution for the off times starting from deep traps surrounding the quantum dots. The depth of the traps is exponentially distributed. And a carrier can only escape the trap when its energy is bigger than the depth of the trap. In this model the transition rate from off to on state is therefore described by a thermal activation function. The probability density of the off times is given by:

$$P(\tau_{off}) = \frac{\alpha k_B T \Gamma(1 + \alpha k_B T)}{A_{\alpha k_B T}} \tau_{off}^{-m} \quad (2.9)$$

with τ_{off} being the duration of the off state and m the exponent of the potential law, that has to be determined experimentally [26].

Other approaches assume that the carriers leave the traps by a tunnelling mechanism [26] or start from fluctuations in the proximity of the quantum dots [28].

2.3 Deep traps and the random telegraph signal

The described blinking behaviors and associated statistics can be caused by different effects. One possible reason can be carriers trapped in localized centres, deep traps. This was reported in a work of Sugisaki *et al* [24]. As our system seems to base on the same mechanism this section will explain the observations of Sugisaki *et al* and its interpretation.

In his work the optical properties of self assembling single InP quantum dots (QDs) were investigated. The InP QDs were sandwiched between two layers of GaInP. When excited with 488 nm light about one per 10^7 QDs showed blinking behavior. Most of these points were found near small flaws. After scratching the sample intentionally the number of blinking points was increased. After Si- δ doping between the QDs and the GaInP cap layer, however, no increase of the number of blinking points could be observed. This suggested that the unstable fluorescence was related to deep traps caused by defects.

At higher temperatures the not blinking points showed lower intensities because of stronger interaction between excitons and phonons at higher temperatures. This increases the nonradiative decay resulting in lower luminescence intensity. This observation could be described by a simple thermal activation model:

$$I(T) = \frac{I(0)}{1 + ae^{-E/k_B T}} \quad (2.10)$$

a is a temperature independent constant, E the thermal activation energy and k_B the Boltzmann constant. The thermal activation energy varied from dot to dot. The blinking InP QDs showed a blinking behavior switching between an on and a off state. The distribution of on and off intervals could be described by a single exponential decay function which is consistent with the quantum jump model explained in section 2.1.

$$N_{on/off}(t) = N(0)e^{-t/\tau_{on/off}} \quad (2.11)$$

$\tau_{on/off}$ are the average on or off times. The difference in intensity between on and off state ΔI was found to vary from dot to dot. Furthermore some points that switch between more than just two levels were found.

Excitation power dependence measurements showed that the switching times of all blinking dots could be fitted with a single exponential function.

$$\tau_P = P^{-\eta} \quad (2.12)$$

P is the excitation power, the exponent η was found to be different for each QD. All these observations proposed a model for the blinking that is based on localized deep traps caused by defects. Carriers can be trapped in the deep localized states. If one of these traps is located near a QD the local electric field generated by the

2.3 Deep traps and the random telegraph signal

trapped carrier impacts on the quantum well and deforms it, the overlap of the electron wavefunction Ψ_e and the hole wavefunction Ψ_h decreases and so does the transition probability and the emission intensity (cf. quantum confined stark effect, section 1.3). After a while the trapped carrier relaxes by recombination with another carrier, mediated by phonons or by photon-reabsorption. The local field is removed and the QD switches back to the on state again. With different distances between traps and QDs the strength of the electrical field in the QD and thus the difference between on and off state intensity $\Delta I = I_{on} - I_{off}$ varies. If there is more than just one trap near the QD the electric fields superpose and the intensity can switch between more than two intensity levels (fig. 2.2). The trapping processes in different traps are independent of each other, therefore any switching between all different intensity levels is possible.

With decreasing temperature the switching got slower and the off times τ_T could be described by a thermal activation function:

$$\tau_T = \frac{\tau_{off}(0)}{1 + ae^{-E/k_B T}} \quad (2.13)$$

a is again a temperature independent constant and E is the thermal activation energy.

2 Random telegraph signal

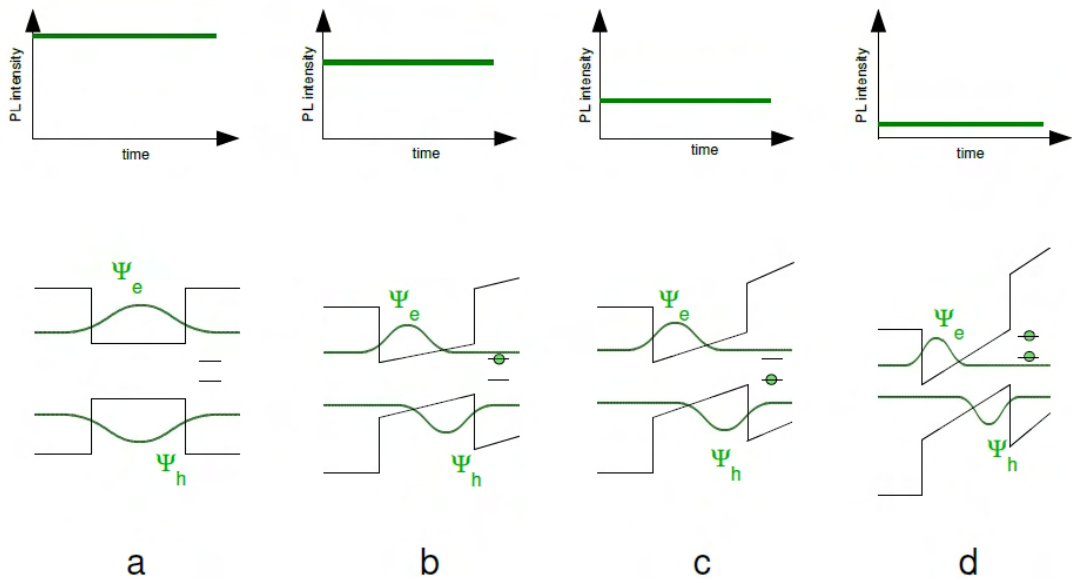


Figure 2.2: Model for the blinking caused by carriers caught in deep traps. (a) shows the quantum well with the electron and hole wavefunctions Ψ_e and Ψ_h and two deep traps. The overlap of the wavefunctions is big and thus the luminescence intensity strong. In (b) a carrier is trapped, the quantum well deformed and the overlap of the wavefunctions reduced. The luminescence intensity gets weaker. (c) shows the effect of a carrier trapped in a trap closer to the QD. The resulting local electric field in the quantum wells is stronger, leading to a bigger deformation and separation of the wavefunctions. In (d) both deep traps are charged, the fields of both charges superpose and the luminescence intensity reaches a minimum. As the trapping and detrapping processes of both traps are independent of each other, the photoluminescence can switch between any of the levels. For a single trap the point switches between only two intensity levels. (after [24])

3 Plasmons and coupling of quantum wells to plasmons

The easiest model for a bulk metal in equilibrium condition describes it as a lattice of ions with a plasma of electrons moving in the Coulomb field of other electrons and ions. When the equilibrium is disturbed by an external electromagnetic field the external field enforces a collective oscillation of the conduction band electrons as the inertia of electrons are much smaller than the ones of the ions. The quantum of such an oscillation is called a plasmon. Although it is a general phenomenon in matter, metals provide by far the best evidence for plasmons, since the conduction electrons in metals can move quasi-free. From the quantum mechanics point of view plasmons are treated like quasi particles.

Oscillating charges are inherently associated with an electromagnetic field. Therefore boundary conditions play an important role in the theoretical description of plasmons and result in the distinction between bulk plasmons (in bulk materials) and surface plasmons (on metal-dielectric interfaces). Surface plasmons are once more subdivided in surface plasmon polaritons and localized surface plasmons. This chapter will introduce to the main characteristics and properties of plasmons with a special focus on the coupling of InGaN quantum wells to surface plasmons in gold films and gold nanoparticles and the enhanced light emission associated with this coupling.

3.1 Bulk plasmons

If the electrons oscillate within a bulk material the plasmons are called bulk plasmons or volume plasmons and describe longitudinal oscillations. The eigen oscillation frequency of the plasma ω_p in bulk metals is called plasma frequency:

$$\omega_p = \frac{Ne^2}{m^*\epsilon_0} \quad (3.1)$$

It depends on the density of electrons N , the effective mass of the electrons m^* , the electron charge e and the permittivity of free space ϵ_0 . This relation can be derived by assuming that the response of the electrons can be described as a simple harmonic oscillator. The phase and amplitude of the plasmon oscillation

in the bulk material relative to the external field depends on the relation of the plasma frequency to the frequency of the driving field [29,30].

3.2 Surface plasmons

Collective excitation modes of the oscillations of quasi free electrons that propagate on the interface of a metal and a dielectric medium are called surface plasmons. Recent literature distinguishes between surface plasmon polaritons and localized surface plasmons [31]. Surface plasmon polaritons propagate on extended interfaces with scales that are much larger than the optical wavelength, whereas localized surface plasmons are confined in geometries much smaller than the optical wavelength. Such geometries can be small metal objects, metallic protrusions, structures, voids covered with metal or metal nanoparticles. For this reason they are often referred to as particle plasmons [31–33].

3.2.1 Surface plasmon polaritons

Surface plasmon polaritons are plasmons that propagate in the interface of a metal and a dielectric medium. This interface is extended and much larger than the optical wavelength. Surface plasmon polaritons are analogous to bulk plasmons with the restriction that they are bound to surface electrons.

The oscillations of the carriers in the interface are accompanied by a longitudinal and transverse electromagnetic field. The field is maximal at the interface and decays exponentially with increasing distance from the interface and is therefore said to be evanescent or called near-field in nature. This behavior is observed in both directions, i.e. the wave is both evanescent in the metal and the dielectric material with different decay rates δ_m and δ_d respectively. Fig 3.1 shows the oscillating charges on the metal dielectric interface and the accompanying fields.

The dispersion relation of surface plasmons, i.e. the dependence of the surface plasmon frequency ω on the wavevector k , shows the change of surface plasmon properties at different frequencies. Fig. 3.2 shows a typical dispersion relation of surface plasmon polaritons. The solid line is the dispersion relation for surface plasmon polaritons in the interface between air and metal, the dashed line between the same metal and a material with higher refractive index than air. The graphs hit asymptotic limits ω_{air} and ω_n with increasing energy. This asymptotic limit depends on the metal and the surrounding material. If the metal is chosen in a way that the resulting asymptotic limit of the surface plasmon polaritons lies in or close to the emission band of the semiconductor the excitons and the surface plasmon polaritons can couple [31].

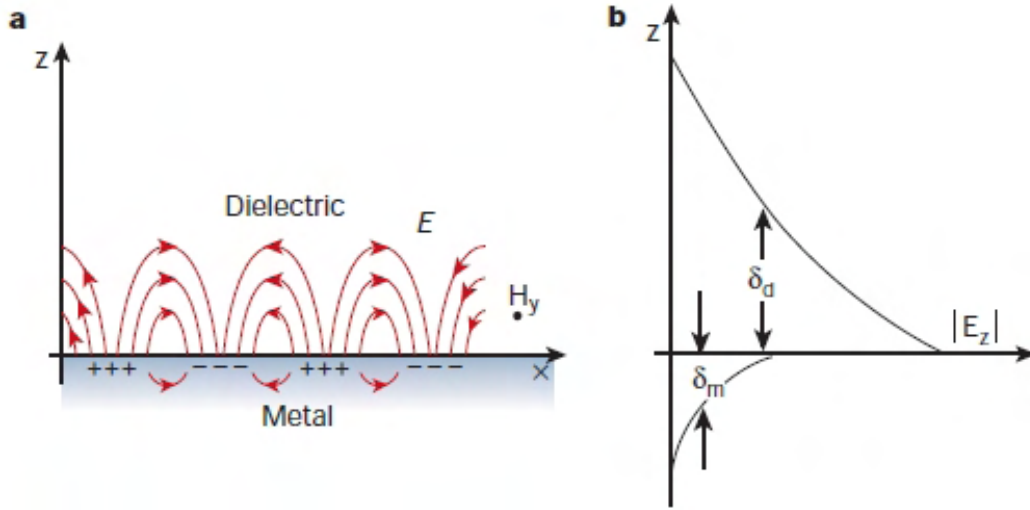


Figure 3.1: (a) Schematic picture of the distribution of oscillating charges on a metal dielectric interface and the fields accompanying them. The magnetic field H_y is transverse. The component of electric field E that is perpendicular to the interface is $|E_z|$. It is evanescent, has a maximum at the interface but decays exponentially both in the dielectric and the metallic medium (b). The decay rate is δ_d for the dielectric medium and δ_m for the metal. (Adapted from [34]).

3.2.2 Localized surface plasmons

Colloidal solutions of nanoparticles of the metals gold, silver and copper show bright intense colors. However these colors can't be observed for the same materials in bulk or individual appearance. The colors are due to particle plasmons excited in the nanoparticles when resonant to the incident light [35]. The fascinating intensive colors of noble metal nanoparticles have historically been of interest in craft work, for example for staining the glass of church windows. Nowadays its optical properties attract much attention due to a variety of exciting scientific applications like biological imaging or sensing, medical photothermal therapy of cancer [36], transport of electromagnetic energy at scales below diffraction limit [33] or the strong enhancement of photoluminescence in quantum wells [37] and more effective LEDs [38], to name a just a few.

In the case of nanoparticles the plasmons are called localized surface plasmons as the plasmons are confined in geometries that are much smaller than the optical wavelength. Localized surface plasmons can also be observed in similar sized metallic structures, objects or voids covered with metal [33]. The confinement in these small areas changes the boundary conditions and with that the resonance conditions.

For the wavelength of the light being much smaller than the diameter of the nanoparticles and for spherical nanoparticles the surface plasmon oscillation mainly dominated by its dipolar mode.

3 Plasmons and coupling of quantum wells to plasmons

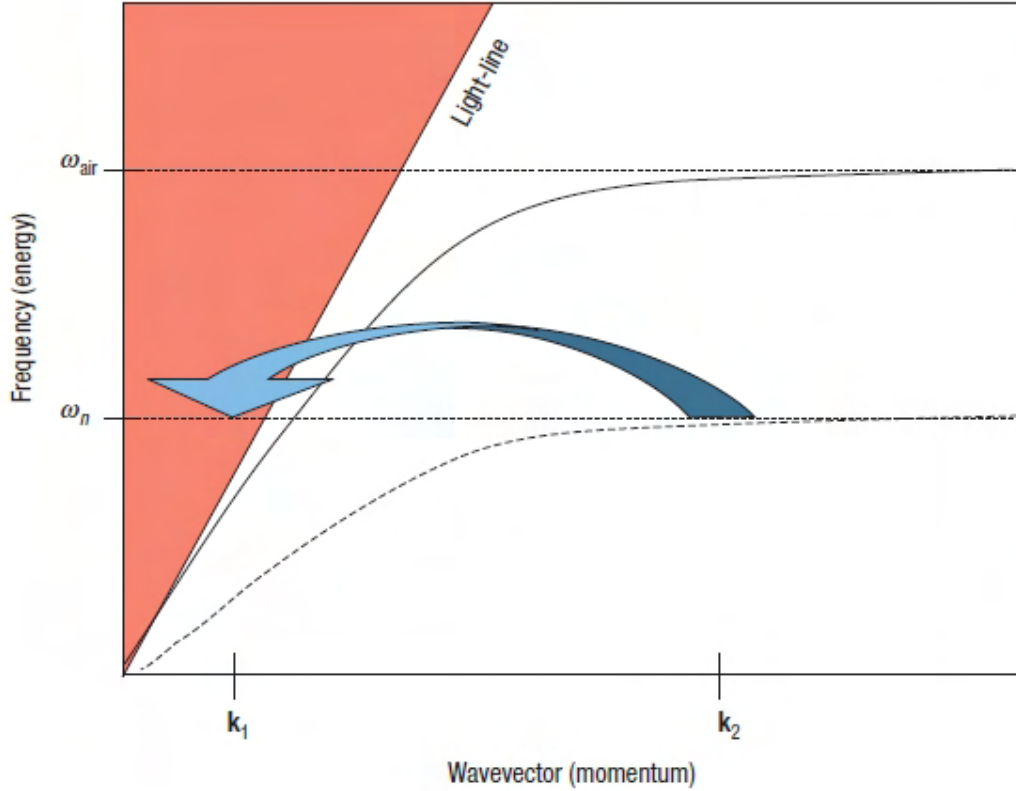


Figure 3.2: Scheme explaining the coupling of the quantum well to surface plasmon polaritons (SPP) and the subsequent coupling of SPP to light (from [31]). The picture shows a typical dispersion relation of SPPs illustrating the relation between the energy (frequency ω) and the momentum (wavevector k). The solid line shows the dispersion relation for an interface between air and metal, the dashed line between the same metal and a material with higher refractive index than air. The graphs hit asymptotic limits ω_{air} and ω_n with increasing energy. This asymptotic limit depends on the metal and the surrounding material. If the metal is chosen in a way that the resulting asymptotic limit lies in or close to the emission band of the semiconductor the excitons and the SPP can couple. If the emission of the quantum well should be enhanced the SPP subsequently have to couple to light which is not possible because the momentum k_2 is too high. A rough surface or periodic structure can scatter SPP of high momentum k_2 to SPP of smaller momentum k_1 (blue arrow). When k_1 lies inside the light-line it can couple to light and emission enhancement gets possible.

3.3 Coupling of InGaN quantum wells to surface plasmons

$$\alpha = 3\epsilon_0 V \frac{\epsilon - \epsilon_m}{\epsilon + 2\epsilon_m} \quad (3.2)$$

α is the polarizability of the dipolar mode, V the particle volume, ϵ_0 the vacuum permittivity, ϵ_m the dielectric constant of the surrounding medium and $\epsilon(\omega) = \epsilon_r(\omega) + i\epsilon_i(\omega)$ the dielectric function of the metal which depends on the frequency and is complex. Strong resonance occurs at the frequency ω where $\epsilon_r = -2\epsilon_m$. This condition is fulfilled for copper, silver and gold nanoparticles at visible wavelengths which makes them suitable materials for a huge variety of applications. The big optical polarization enhances the electrical field strongly at particles surface and causes a strong enhancement of scattering and absorption of the electromagnetic waves at resonance frequency [39].

The resonance frequency depends on the size and shape of the nanoparticle, the metal, the dielectric constant of the surrounding medium and interactions caused by the coupling between different nanoparticles. All this makes the resonance frequency tuneable and therefore interesting for lots of biological and medical applications [36].

The size dependence of gold nanoparticles in water was shown in a study of Link et al [35] by the absorption spectra of particles of different sizes (fig. 3.3). Its maximum blue-shifts with decreasing particles size. For gold nanoparticles with diameters of 9, 22, 48 and 99 nm the absorbance maxima are located at $\lambda_{max} = 517, 521, 533$ and 575 nm. Compared to this the temperature dependence of the plasmon resonance for gold nanoparticles is very small [35]. For our experiments where a InGaN/GaN single quantum well of 540 nm central emission coupled to surface plasmons, we chose gold nanoparticles of 50 nm diameter. The resonance maximum of the 48 nm gold nanoparticles (fig. 3.3) is located at 533 nm. So 50 nm gold nanoparticles were likely to show resonance to our sample (cf. section 4).

3.3 Coupling of InGaN quantum wells to surface plasmons

If a metal is chosen in a way that its plasmon frequency matches the emission spectrum of a quantum well, this metal can be placed on the quantum well and the quantum well resonantly couples to surface plasmons. The electron hole pairs transfer their energy to surface plasmons in the semiconductor metal interface via the evanescent field instead of radiating it into free space [40,41].

This coupling has been observed in a study of Okamoto et al [37]. They observed large enhancements in the emission of InGaN/GaN quantum wells after putting silver or aluminum layers 10 nm above the InGaN layer (fig. 3.4). This enhancement was attributed to the energy transfer from the quantum well to surface plasmons in the GaN-metal interface and the subsequent increase of the density

3 Plasmons and coupling of quantum wells to plasmons

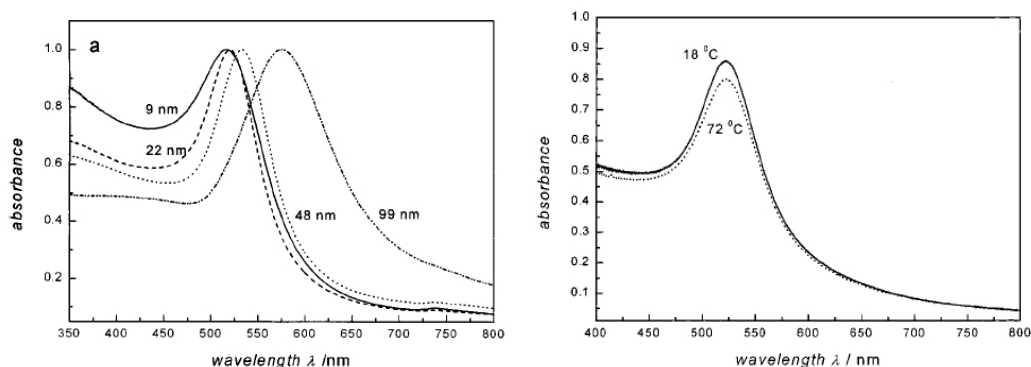


Figure 3.3: The absorption spectra of gold particles of 9, 22, 48 and 99 nm diameter in water, normalized at their absorption maxima (left). The absorption spectra of gold nanoparticles of 22 nm diameter in dependence of the temperature at 18 °C and 72 °C (right). (both images from [35])

of states and spontaneous emission rate.

In studies of Gontijo et al [42] the surface plasmon-quantum well coupling manifested itself in an suppression of the emission. A spectral sharp photoluminescence dip was observed after a 8 nm silver layer was placed 12 nm from a InGaN/GaN quantum well. The spontaneous emission into surface plasmons was 55 times faster than the normal spontaneous emission of a InGaN quantum well into free space. Time-resolved photoluminescence measurements conducted in a study of Neogi et al showed that the enhanced spontaneous emission into surface plasmons was even 92 times faster [40].

As described in section 3.2.1 the surface plasmon electromagnetic field is evanescent and exponentially decays with increasing distance from the metal semiconductor interface. Only electron hole pairs in the near-field of the surface can couple to surface plasmons. For resonant coupling the active InGaN layer has to be placed within the fringing field penetration depth of the electromagnetic field. The penetration depth of the surface plasmon fringing field into the semiconductor is given by:

$$Z = \frac{\lambda}{2\pi} \left(\frac{\epsilon'_{GaN} - \epsilon'_{metal}}{\epsilon_{GaN}^2} \right)^{1/2} \quad (3.3)$$

ϵ'_{GaN} and ϵ'_{metal} are the real parts of the dielectric constant of GaN and the metal respectively. For Ag this calculation leads to a penetration depth Z of 47 nm, for Al 77 nm and for the case of Au 33 nm [37]. For this reason the thickness of the GaN cap layer is crucial and can decide whether a quantum well couples to surface plasmons or not.

In the studies of Neogi et al the resonance strongly depends on the thickness of the Ag layer [40]. In the case of nanoparticles coupling is stronger in areas with

3.4 Coupling of surface plasmons to light

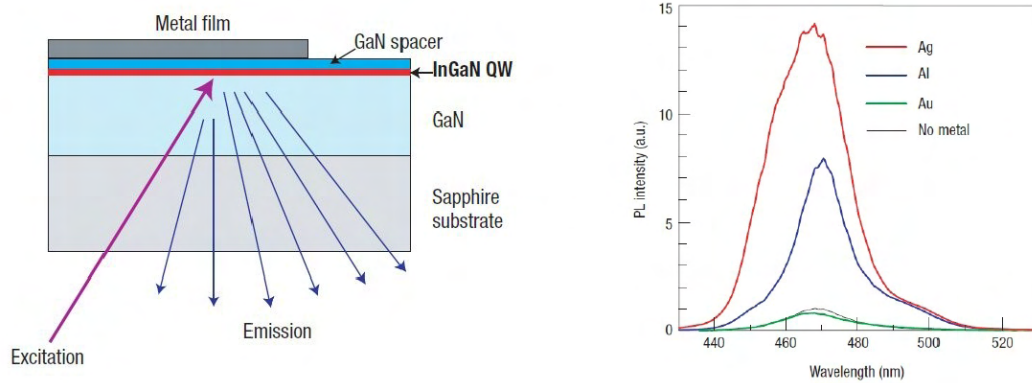


Figure 3.4: Okamoto et al showed that the photoluminescence of InGaN quantum wells can significantly be enhanced through a thin metal layer over the GaN cap layer (left). The black line shows the photoluminescence spectrum of the quantum well without metal. A thin film of aluminum (blue line) or gold (red line) caused a strong emission enhancement (right) (both images from [37])

high density of nanoparticles than in an area with less particles because of the bigger number of coupled surface plasmon modes. [43].

3.4 Coupling of surface plasmons to light

The coupling between quantum wells and surface plasmons can either enhance or suppress the light emission efficiency depending on if and how strong the surface plasmons couple to light. In the studies of Gontijo et al the surface plasmon quantum well coupling manifests itself in a suppression of the emission, whereas the studies of Okamoto et al show an enhancement in the emission. However, in both cases the quantum well resonantly couples to surface plasmons [42, 44]. In one case the surface plasmons subsequently couple to light and the energy is radiated into free space, in the other case the energy of the surface plasmons is absorbed in the metal.

Usually the probability of losing energy through surface plasmons in LEDs is high. For most LEDs a metal contact has to be put near the the semiconductor layer, causing high probability for the excitons to couple to surface plasmons. The plasmons are unable to generate light directly due to their high momentum. The energy lost to the surface plasmons is dissipated as heat and the efficiency of the LED decreases [31]. In this case the plasmons decay in electron hole pairs. This can happen intraband or interband then being converted in heat through electron-electron and electron photon relaxations [36].

3 Plasmons and coupling of quantum wells to plasmons

Surface plasmons have a smaller wavelength for the same frequency of a photon. Therefore they cannot couple directly to free-space electromagnetic radiation of the same energy, their associated wavevector being too large to satisfy conservation of energy and momentum. To couple surface plasmon polaritons to light the momentum mismatch between light and surface plasmon polaritons must be bridged i.e. both the frequency and wavevector of the surface plasmons and the light must match. If the surface plasmons are scattered and thus loose momentum the resulting momentum can match the momentum of the light (fig. 3.2) and the surface plasmon polaritons can thus couple to light and enhance emission. The surface plasmons can be scattered at suitable periodic structures [31, 34, 41, 45] Okamoto et al use a similar method to achieve the scattering of the surface plasmons. Instead of introducing a periodic structure they observed that only the inherent surface roughness and imperfections of the evaporated film can efficiently scatter surface plasmon polaritons and increase the coupling to light [37]. For nanoparticles the inherent curvature itself causes relaxation of the k selection rule for plasmons and the coupling of the particle plasmons to light is increased [46, 47].

Kwon et al reported on the first realization of a GaN based LED structure with quantum well surface plasmon coupling. These structures were realized by inserting a Ag nanoparticle layer between the n-GaN layer and the multiple quantum well. By this it was possible to enhance the emission through the coupling to surface plasmon and to maintain the p-n junction. [38]

3.5 Quantum confined stark effect screening vs. surface plasmon coupling

The main reason for the emission enhancement in InGaN/GaN quantum wells is the coupling of the quantum wells to surface plasmons and the subsequent light emission. But also screening of the QCSE through the electric fields of the surface plasmons plays an important role in the enhancement process. This screening both influences on direct emission and on the coupling strength between quantum well and surface plasmons. First, the screening undoes the QCSE itself leading to increased recombination probability of electrons and holes. Second, the screening shifts the emission spectrum back to smaller wavelengths. This way the emission spectrum can get closer or farther away from the surface plasmon resonance energy resulting in higher or lower densities of surface plasmon states and thus in stronger or weaker quantum well surface plasmon coupling [41].

3.6 Plasmons in nanoclusters of metallic indium

During the growing process of InN it tends to spontaneously precipitate cluster-like metallic indium particles. There are several evidences that these metallic indium clusters are plasmonically active. For example the fluorescence of organic materials located near indium clusters was significantly enhanced or the electroluminescence of Si with In clusters increased strongly due to coupling to plasmons in the metallic indium particles. Comparisons between cathodoluminescence and SEM images of a InN film with In clusters demonstrated strong emission enhancement at the locations of the indium particles. The metallic indium clusters in the InN film could both enhance the emission or absorb. Which effect appears depends on the form, orientation and quality of the clusters [33]. This effect is very similar to the emission enhancement and suppression reported in the studies of Okamoto et al [37] and Gontijo et al [42] where the interaction of a InGaN/GaN quantum well with surface plasmons in metal films was investigated on.

Part II

Experiments

4 Samples

The samples used for the experiments of this thesis were InGaN/GaN quantum wells grown on an (0001) oriented sapphire substrate by metalorganic chemical vapor deposition technique developed by Nichia Chemical Industries Ltd., Japan. All the samples were single quantum well structures composed of an undoped GaN layer (4 μm), an $\text{In}_x\text{Ga}_{1-x}\text{N}$ active layer (3 nm) and a undoped GaN cap layer (5 nm) (fig. 4.1). Four different samples with different indium concentrations x , resulting in different photoluminescence spectra, were used. The main emission peaks were located at 540 nm, 510 nm, 460 nm and 420 nm (fig. 4.1) at 365 nm excitation wavelength and roomtemperature.

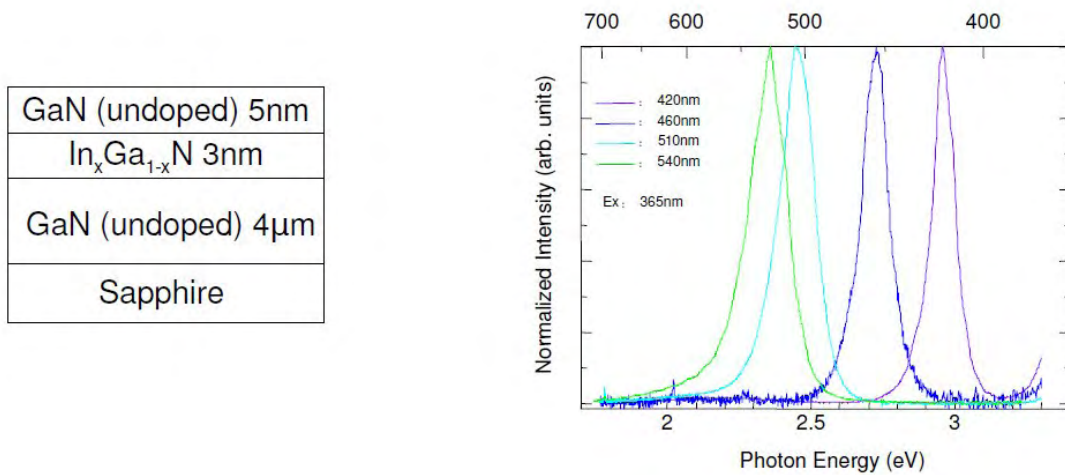


Figure 4.1: The structure of the four samples grown on a sapphire substrate with a 4 μm GaN layer, a 3 nm InGaN active layer and a 5 nm cap layer (left). Different Indium concentrations x result in different emission spectra with main emission peaks located at 420, 460, 510 and 540 nm (right).

The samples could be excited with the 365 nm or the 435 nm line of a mercury vapor lamp. The band gap of GaN is about 3.4 eV (365 nm) and the one of InGaN is under 2.95 eV (over 420 nm). The 365 nm line therefore excited both the GaN barrier and the InGaN active layer [3].

At 365 nm excitation the photoluminescence showed points of very high intensity. Fig. 4.2 shows the emission patterns of the 460 nm, the 510 nm and the 540 nm sample. On all samples intense luminescent centres could be observed, some

4 Samples

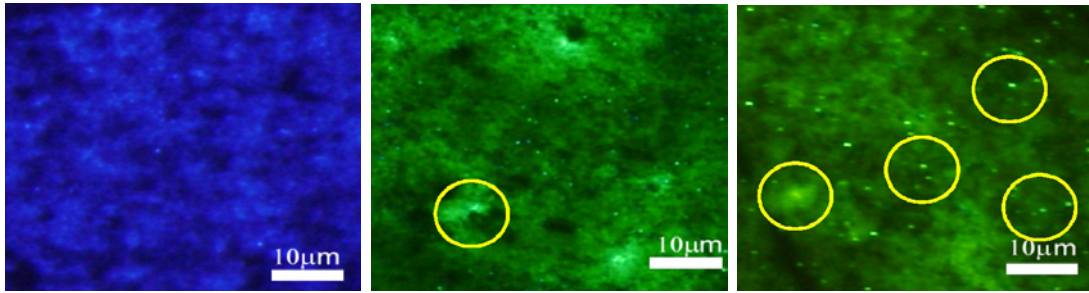


Figure 4.2: The photoluminescence of the samples with 460 nm, 510 nm and 540 nm main emission peak (from left to right) at 365 nm excitation. All samples show intense emitting centres. The yellow circles mark blinking points. With increasing indium concentration more blinking points can be observed.

of these bright points blinked. Most blinking points could be found on the 540 nm sample, less on the 510 nm sample and no blinking points could be observed on the blue emitting 460 nm sample. Excited with 435 nm none of the samples showed intense emitting centres or blinking points.

5 Time intensity profiles

In contrast to normal intense luminescent centres blinking points change emission intensity. In order to investigate on the blinking behavior time-intensity profiles had to be plotted and analyzed. This chapter will explain the methods to provide and analyze such time-intensity profiles and the results obtained from them.

5.1 Method

The experimental setup to get the time-intensity profiles of the blinking points consisted of a photoluminescent microscope coupled with a CCD camera. Movie files of the photoluminescence of the sample were taken and processed with different scilab programs to analyze the blinking behavior.

The Olympus photoluminescent microscope BX51WI was used with different Olympus objectives of the LMplanFLN series with 10x, 20x and 50x enlargements. The videos for the time-intensity profiles were taken with 50x enlargement. The samples were excited by the mercury vapor lamp Olympus U-LH 100HQ. With filters the exciting wavelength could be switched between 365 nm and 435 nm.

To record the videos two different cameras were used, a Sony HDR-SR1 which provided a framerate of 30 fps and a Casio EX-F1 that could be operated in high speed mode with framerates of 300, 600 or 1200 fps. Operating the camera in 600 fps and 1200 fps mode turned out not to deliver good results. The light sensitivity got too low so that even the brightest points could hardly be seen on the video. As the cameras were conventional ones and not particularly designed for the microscope, for the Sony camera the Olympus ocular UIS2 WHN 10x/22 was used as a adapter. For the Casio camera a simple plano-convex lens with focal length of $f=100$ mm replaced the adapter.

In most experiments the Sony camera was used. It only had a framerate of 30 fps and therefore was much slower than the second camera which in high speed mode could achieve framerates of 300, 600 and 1200 fps. The slower camera was easier to operate, as the correct alignment of the focus could be checked on a monitor. Whereas with the highspeed camera the focus could only be aligned using the integrated display which in most cases resulted in videos of bad quality. Furthermore the light sensitivity of the high speed camera got very low with increasing framerate and the noise got very high. In the 300 fps mode it still

5 Time intensity profiles

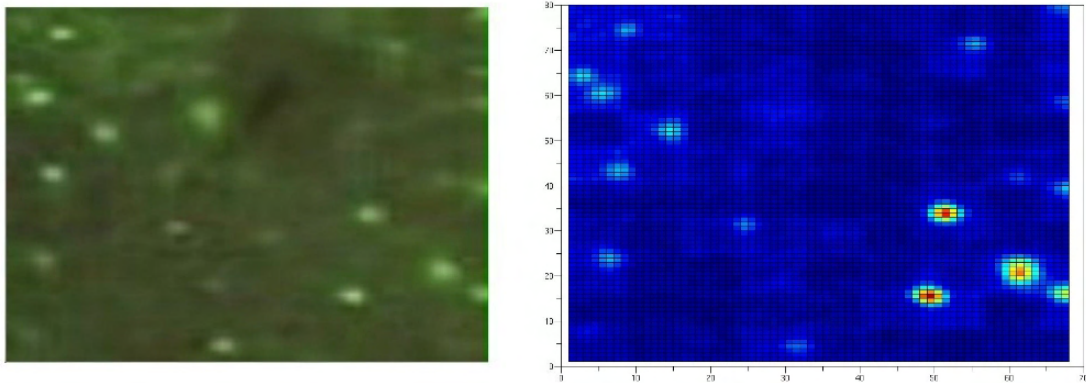


Figure 5.1: To locate the blinking points, for each pixel of the movie file the standard deviation of the intensity was calculated. The left picture shows the photoluminescence of the sample, the right picture shows the corresponding color-coded map of standard deviation calculated from the movie file. Red points show pixels with high standard deviation, blinking points, blue pixels designate not blinking areas.

delivered good results only for the brightest blinking points (fig. 5.3), but weaker blinking points could not be observed anymore. At 600 fps and 1200 fps the light sensitivity got too weak to obtain meaningful results.

In order to analyze the temporal behavior of the blinking points different scilab programs were used to process the avi-format movie files that had been taken of the blinking points. The movie files delivered 3 different intensity values (blue, red, green). As the blinking points were green, the other channels didn't provide any further information. For this reason and to save computing time just the green channel was used. The movies were cropped and the intensity values of each frame and pixel were used to calculate the standard deviation of each pixel. Mapping the standard deviation (fig. 5.1) made it possible to localize the blinking points. The red points in fig. 5.1 show pixels with high standard deviation (blinking points), blue points show pixels with low standard deviation (not blinking). After rechecking with the movie file a suitable blinking point was selected and the time intensity profile of this point was extracted. As a blinking point consists of more than one pixel the intensities of the pixels belonging to one blinking point were summarized. With knowing the framerate the timescale could be calculated and the time-intensity profile plotted. Fig. 5.2 shows two time-intensity profiles of a blinking point and of a not blinking area in its vicinity.

Errors caused by the camera could be minimized by setting off a not blinking area against the blinking point. But the fluctuations of the not blinking area turned out to be quite small compared to the blinking (fig. 5.2). Therefore in most cases just the blinking points were taken into account regardless of a reference area. At the University of Regensburg Anne Kuhnert took the time-intensity profiles of blinking points using a photomultiplier reaching a sampling rate of 1-10 kHz [15].

5.2 Different types of blinking points

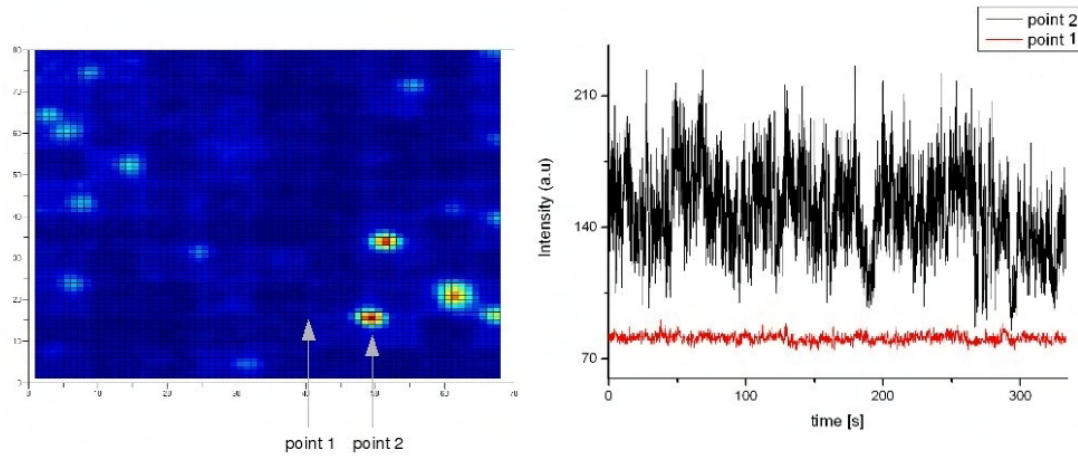


Figure 5.2: The left side shows a color-coded map of the standard deviation permitting the localization of blinking points. The right side shows examples for time intensity profiles of a blinking point (point 2) and a not blinking area in the vicinity of the blinking point (point 1).

The time resolution of the here described method is much lower (30 fps for standard mode camera, 300 fps for high speed camera) and a lot of postprocessing had to be done. On the other hand, measurements that can not be done with the photomultiplier are possible with the camera (e.g. temperature dependence measurements). In spite of the lower timeresultion we could analyze the statistic of the blinking and verify that the blinking is subject to the quantum jump model statistics. The blinking point we observed for this purpose blinks slower than the ones of the samples used at the University of Regensburg. Furthermore the noise was very small compared the distance of the two intensity levels and even without digital filters meaningful results could be obtained.

5.2 Different types of blinking points

On the basis of the time intensity profiles different kinds of blinking points could be characterized. The first type switching between two different intensity levels ('two level blinking point'). For such points clear on and off states could be defined and the times spent in the on and accordingly in the off state could be counted and the two level blinking points could be assigned to different blinking statistics. The second type of blinking points showed more than two intensity levels or didn't show discrete intensity levels at all ('multi level blinking point').

5 Time intensity profiles

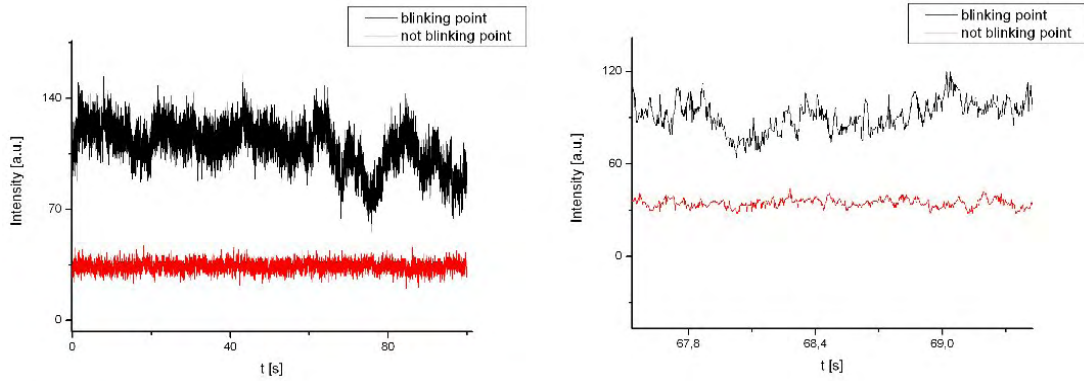


Figure 5.3: Example for a time intensity profile calculated from a movie of a camera operating in high speed mode. This way framerates of 300 fps could be achieved.

5.2.1 Two level blinking points

A very small amount of the blinking points showed two discrete intensity levels. The intensity of these points switched between these two levels and clear on and off states could be defined (fig. 5.4). A intensity histogram illustrates the on and off states of the random telegraph signal and facilitates the selection of a limit between the on and the off state (fig. 5.5). The difference $\Delta I = I_{on} - I_{off}$ between the intensities of the on state I_{on} and the off state I_{off} and the speed of the blinking varied for different two level points.

Using a scilab program the timeintervals spent in the off or the on state could be counted. The probability distributions revealed two different kinds of statistics.

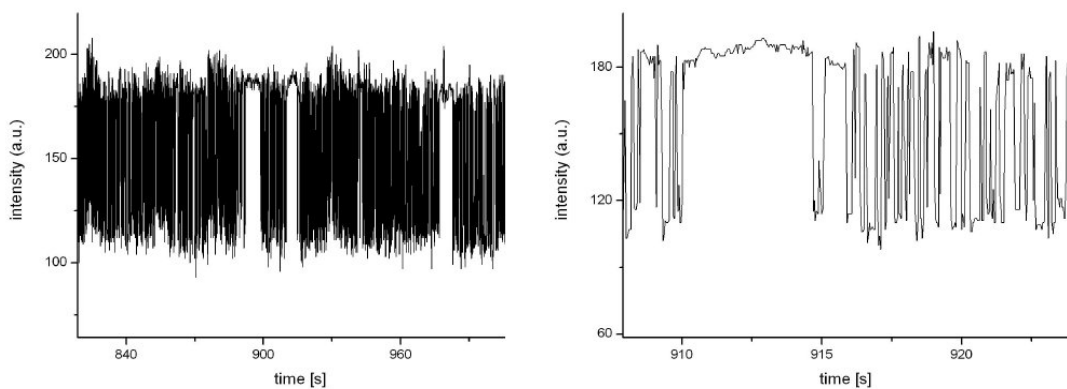


Figure 5.4: The time intensity profile of a two level blinking point. The intensity switches between two states, a on and a off state.

Some two level blinking points show exponentially distributed probabilities of

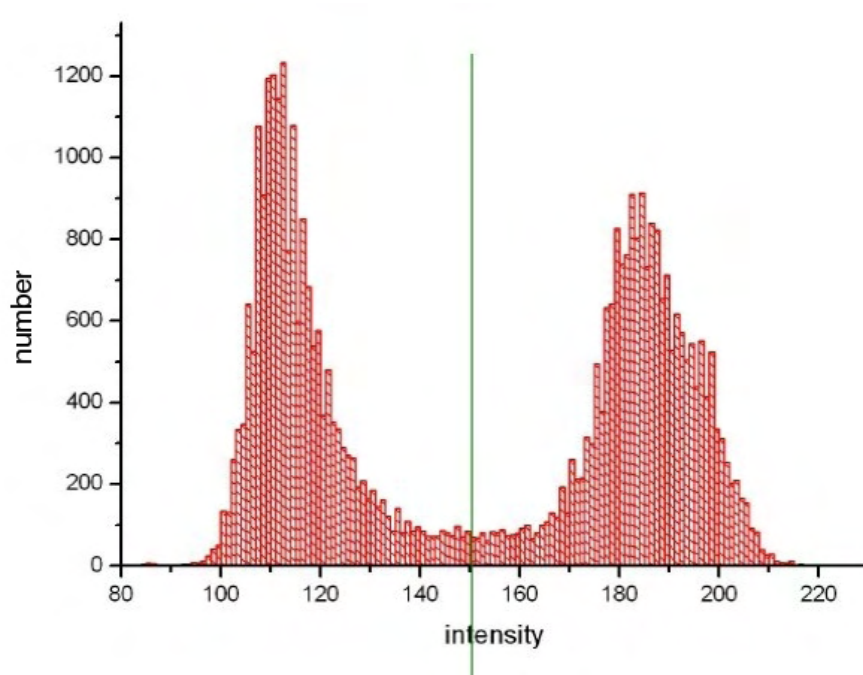


Figure 5.5: The intensity histogram of a 30 min measurement reveals that the intensity only switches between two levels. By means of these histograms limits between a on and a off state could be determined and the on and off times could be counted.

on and off intervals (fig. 5.6). This indicates that the blinking is caused by a quantum jump like mechanism as described in section 2.1.

By contrast other two level blinking points were found that didn't show exponentially distributed probabilities of on and off times (fig. 5.7). The probability distributions of these points could be described by a power law (section 2.2) which indicates a more complex underlying process than a quantum jump. Earlier works conducted with the same samples at Kyoto University [3] reported on this kind of random telegraphic blinking but did not find blinking points with exponential probability distributions.

5.2.2 Multi level blinking points

Besides the very rare two level blinking points most blinking points on the 540 nm sample switched between more than two levels or did not show clear intensity levels at all. Fig. 5.8 shows the time intensity profile of such a multi level blinking point. As for such points clear intensity levels could not be observed in the histogram no states could be defined and statistics on this kind of blinking were not possible (fig. 5.9). In section 6 a multi level blinking behavior could be simulated as a superposition of several two level blinking behaviors.

5 Time intensity profiles

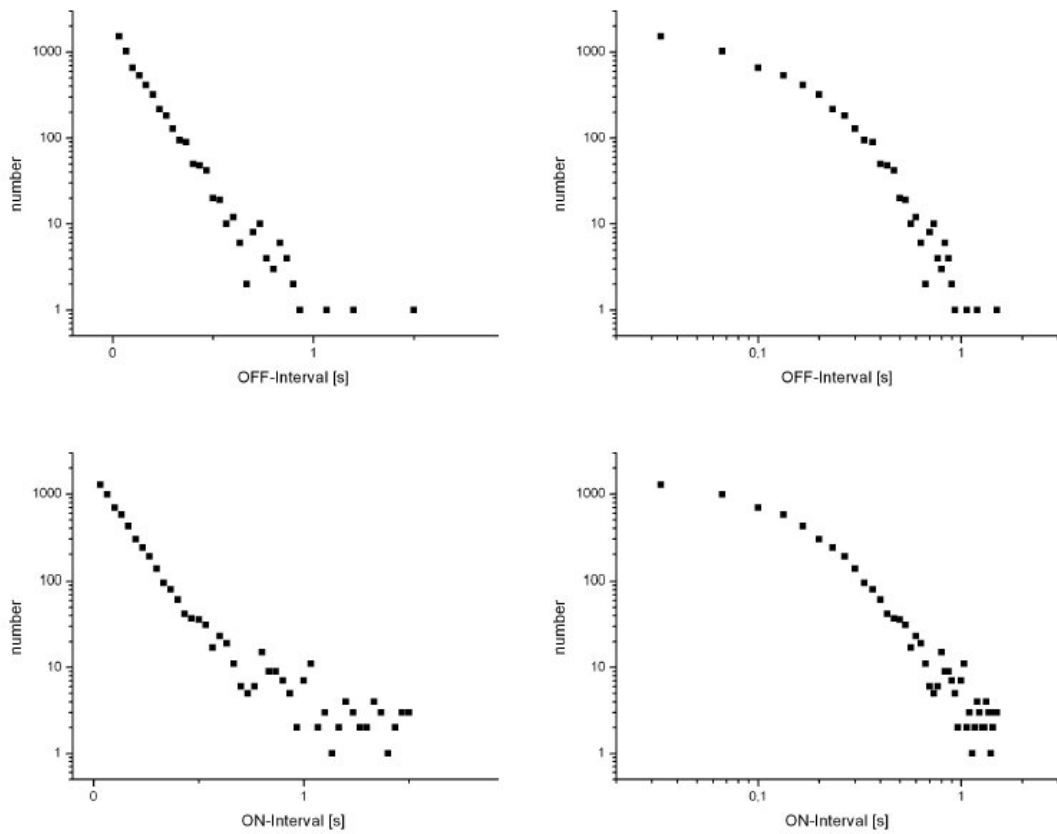


Figure 5.6: Counting the on and off times shows an exponential probability distribution of on and off times. Thus this distribution can be described by the quantum jump theory.

5.2 Different types of blinking points

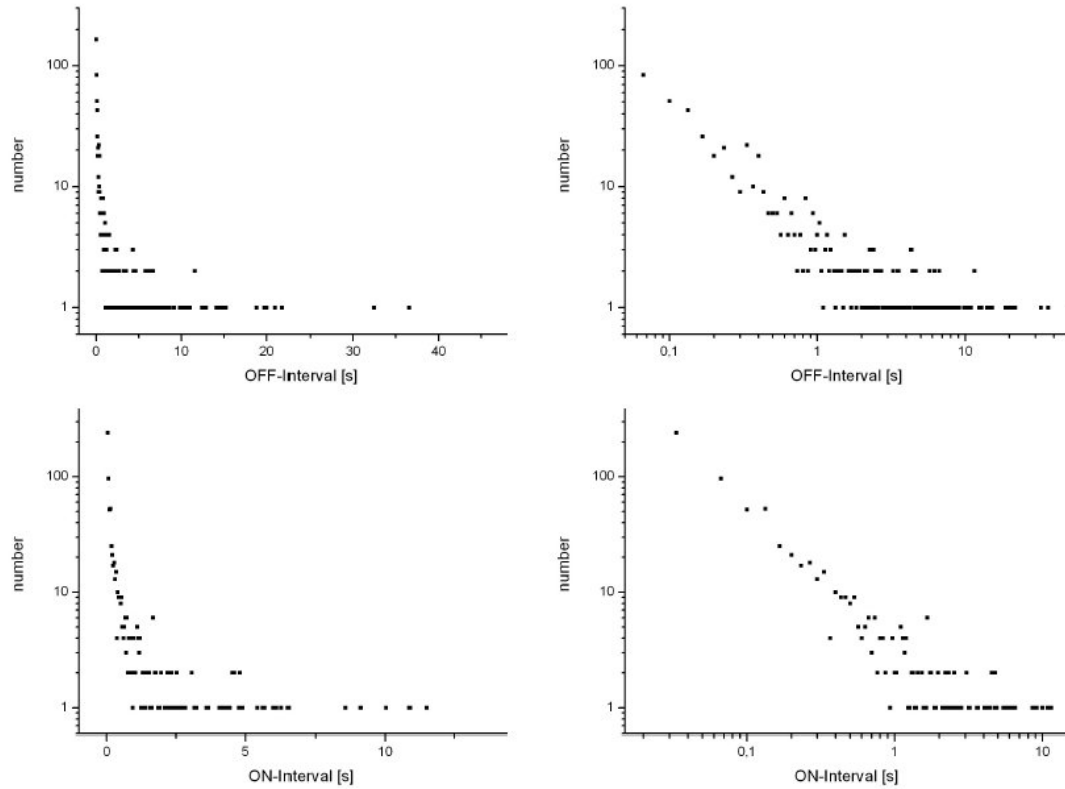


Figure 5.7: Counting the on- and off-intervals of the blinking points shows a distribution that can be fitted with a straight line when plotted on double logarithmic axes (right) but not when plotted single logarithmically (left). This indicates a power law distribution.

5 Time intensity profiles

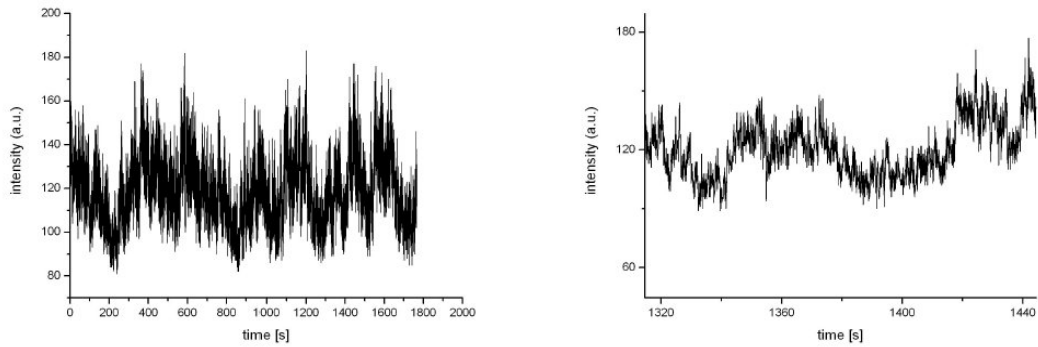


Figure 5.8: The commonly encountered type of blinking point is a multi level blinking point. In the time-intensity profile no discrete intensity levels can be identified.

5.2.3 Interpretation

We think the three different kinds of blinking described in this chapter all base on the same underlying mechanism, which can in the easiest case be described by the quantum jump mechanism. Deep localized states can act as traps for carriers. Trapped carriers cause a local electric field deforming the quantum wells. If such a trapped carrier is located in the vicinity of a strongly light emitting center it can change the transition probability and thus the emission intensity of such a bright dot either through strengthening or screening the quantum confined Stark effect. When the carrier escapes the trap the local electric field impacting on the intensity of the bright dot is removed. This way the trapping and detrapping of a carrier in a localized state can cause a random telegraph signal. This process is illustrated in fig. 2.2. A blinking caused by this process shows exponentially distributed probabilities of on and off times (section 2.1).

Different distances of a trap to an intense light emitting center result in different strengths of the local electric field and thus in different changes in the photoluminescence. The two level blinking points observed for this work showed different distances $\Delta I = I_{on} - I_{off}$ between the on state intensity I_{on} and the off state intensity I_{off} . The same observations were made for blinking points in InGaN/InGa multi quantum wells in the work of Anne Kuhnert at the University of Regensburg [15].

The other two kinds of blinking points which are the two level points with power law probability distributions and the multi level points are probably due to more complex situations. The coupling of a strong light emitting center to more than one trap leads to a superposition of several local electric fields and thus to a more complex blinking behavior like the one of a multi level blinking point. Most of the blinking points on the sample used for this work showed multi level blinking behavior. Two level blinking points were extremely rare and hard to find. In contrast the blinking points in Regensburg all switched between only two intensity

5.2 Different types of blinking points

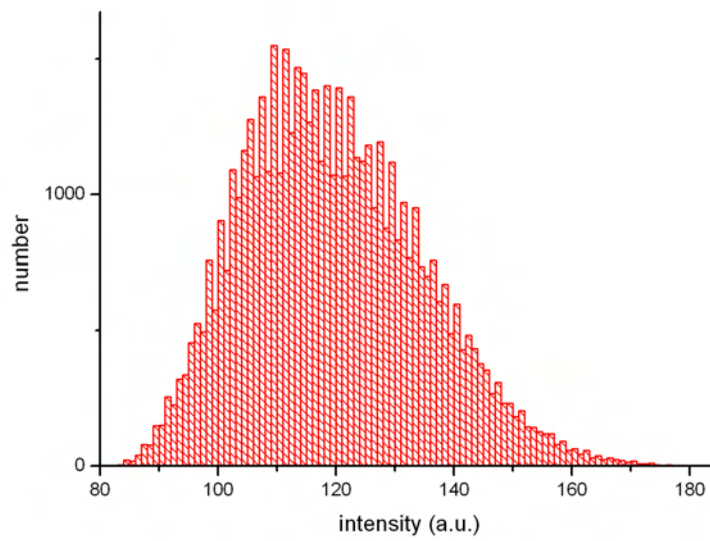


Figure 5.9: In the intensity histogram for a multi level blinking point no discrete intensity levels can be observed.

levels [15].

6 Simulations

We think the three different kinds of blinking are all caused by a fundamental blinking behavior being the two level blinking described by the quantum jump theory. Both the multi level blinking and the two level power law blinking are due to more complex situations i.e. the coupling of one blinking point to more than just one deep trap. Anne Kuhnert characterized the behavior of blinking points of a InGaN multi quantum well at the University of Regensburg. On this sample only blinking points switching between two intensity levels could be found. Furthermore all these points showed quantum jump statistics [15]. To check if a multi level blinking behavior can result from a superposition of different quantum jump two level blinking points, a simulation similar to the one in [15] was performed.

First the blinking of a point that just couples to one single deep trap and follows the quantum jump statistics was simulated. For this a array of uniformly distributed random numbers x was generated. This numbers can be transformed into exponentially distributed random numbers by:

$$t = -\ln(x)/b \quad (6.1)$$

The new array of exponentially distributed numbers corresponds to the on/off times in in the quantum jump model. Two arrays like this where generated, one for the on-, one for the off times, each with different decay rate b . The two intensities I_1 and I_2 were determined and incorporating the camera framerate and the timeintervals intensity datapoints could be calculated.

A multi level blinking point that couples to more than just one deep trap was seen as a superposition of two level quantum jump blinking behaviors. The resulting multi level blinking point switches between maximal $n_{level} = n_{trap}^2$ levels, where n_{trap} is the number of deep traps it couples to. The number of traps, the caused intensity differences and the decay times could be chosen and data points could be simulated for each single trap. A superposition led to the data points of a multi level blinking point.

This simulates the blinking behavior, but still without noise. The noise of the measurements showed gauss shaped distributions. This was simulated with the Box Muller transform [48, 49] which takes two arrays of uniformly distributed random numbers x_1 and x_2 and calculates an array of normally distributed random numbers x by:

$$x = \sqrt{-2 \ln x_1} \cos 2\pi x_2 \quad (6.2)$$

6 Simulations

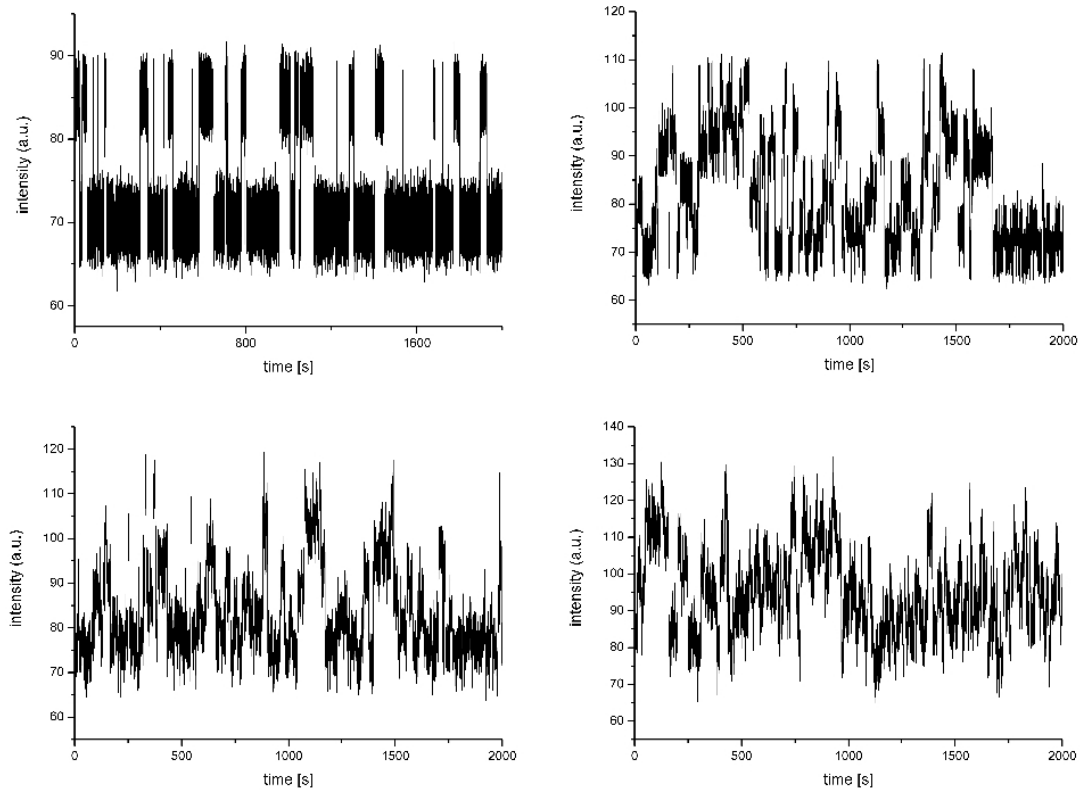


Figure 6.1: Simulated data for blinking points calculated on the basis of the quantum jump theory. Superposing different two level points leads to a blinking behavior where clear levels are not longer observable. The graphs show the simulated data for a blinking point coupling to 1 trap (top left), 3 traps (top right), 5 traps (bottom left) and 10 traps (bottom right).

This way a noise value was generated and added to each data point.

The evaluation of the simulated data was done the same way than that of the measured data. In the simulation the number of traps and the depth and probabilities of on and off state of each trap can be varied. Changing this parameters has a strong influence on the shape of the time-intensity-profile and the histogram. Starting from a two level blinking system with only one trap, adding more traps leads to a blinking behavior that doesn't show clear intensity levels anymore (fig.6.1). This way, data for a multi level blinking point that are very similar to the measurements could be simulated (fig.6.2).

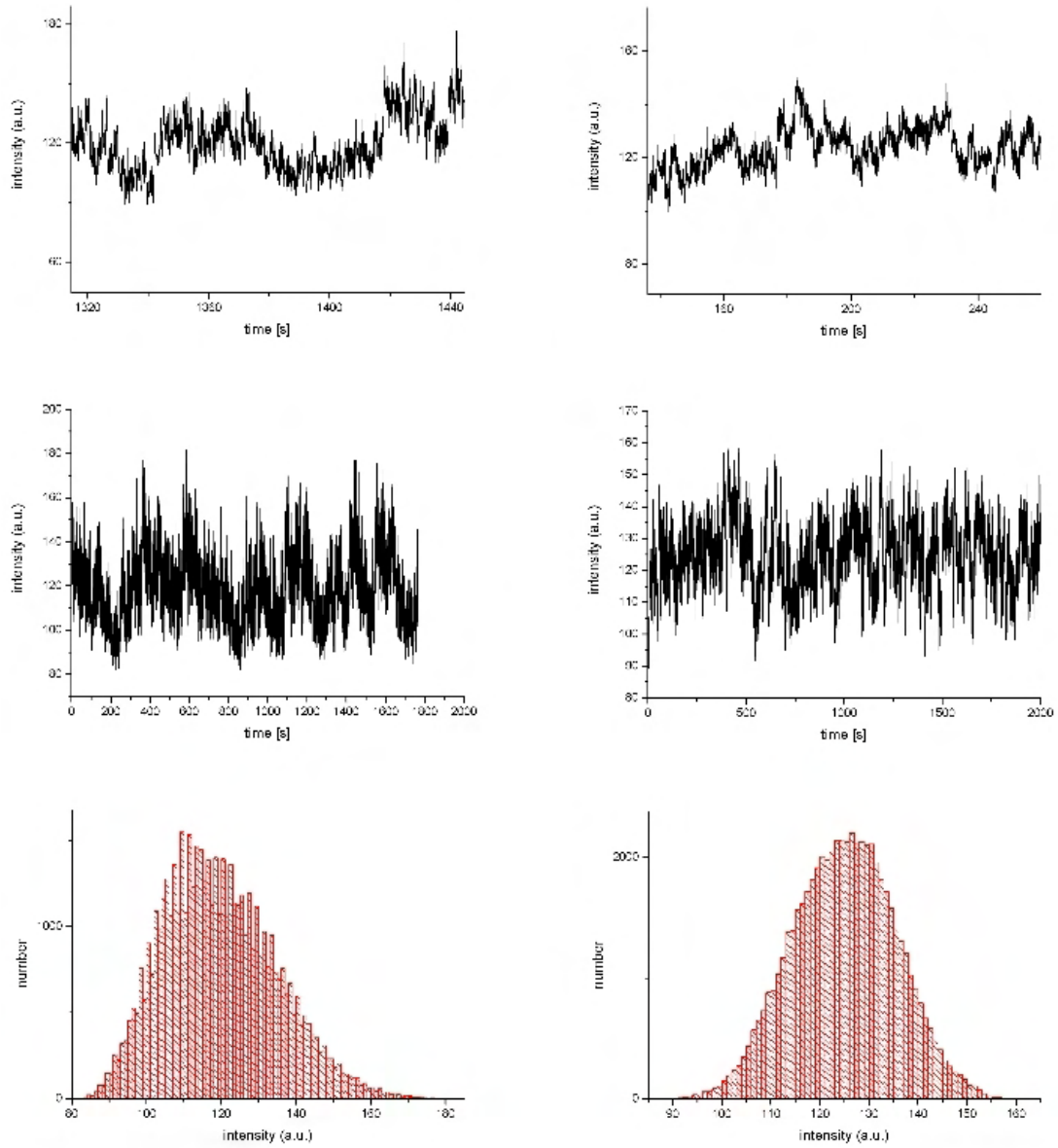


Figure 6.2: Time intensity profiles and histograms of a multi level blinking point. The left side shows measured data, the right side simulated data. For the simulation 10 two level blinking points were superposed, each of the points having other parameters and coupling strength.

7 Temperature dependence of the blinking

7.1 Method

For the temperature dependence measurements the microscopy cryogenic workstation RC102-CFM of Cryo Industries of America Inc. was used. The Model 32 B Cryogenic Temperature Controller permits the maintenance of stable temperatures.

For making statistics on two level blinking points like in section 5.2.1 long movies of 30 minutes had to be taken. The observed area drifted about 10 pixels in this time. This shift couldn't be observed at room temperature and was therefore probably due to vibrations of the cryostat pumps. To compensate this shift the position of the relevant blinking point was localized by mapping the standard deviation beginning with the first frame, then every 5 minutes and in the last frame. This way the point could be traced and its 'route' could be identified. To get the time intensity profile of the blinking point the intensity values of all pixels passed by the blinking point were summarized. The area just contained one blinking point and the statistics depend only on the time intervals spend in the on and the off state and not on the intensity values of the on and off states. This summarizing led to time intensity profiles of a two level point like the ones observed in section 5.2.1.

On the basis of the associated intensity histogram a limit between on and off state could be set and the probability distribution of times spend in the on and off state could be determined. For this purpose it is important to normalize the data in terms of the number of on and off events. All measurement periods took 30 minutes but at lower temperatures the blinking gets slower and the number of switching events smaller. This had to be considered when comparing statistics on the on and off times at different temperatures.

The analysis of the temperature dependence of multi level blinking points was quite easy as almost all blinking points showed this behavior. In contrast two level blinking points were very rare and hence hard to find. Furthermore, after some 30 minutes measurements of the same point at different temperatures this point often changed blinking behavior i.e. it switched off completely or turned into a multi level blinking point. For this reason it was only possible to analyze the

7 Temperature dependence of the blinking

temperature dependence of one blinking point obeying the power law distribution at temperatures ranging from 315 K to 275 K.

7.2 Photoluminescence changes

Fig. 7.1 shows photoluminescence images of the same area on the 540 nm central emission sample at different temperatures beginning from 310 K down to 80 K in steps of 10 K. The right half of the images appears very bright compared to the left half. The right half is covered with a thin gold film that strongly enhances the emission of our sample through resonant coupling of the quantum well to surface plasmons in the gold film. This effect will be described in detail in section 8. This emission enhancement lets the strong light emitting points and thus the blinking points disappear in a uniformly bright emitting area. Therefore no blinking points can be observed on the right half. The left half however shows blinking points. With lower temperatures these blinking points blink slower, get weaker and finally disappear. With decreasing temperatures the quantum well as a whole gets brighter. As the probability for non radiating transition decreases the efficiency of the quantum well increases.

7.3 Two level blinking points

30 minutes movie files of the same two level blinking point were taken at different temperatures in the range from 315 K to 275 K. A comparison of the time intensity profiles at different temperatures shows that the off intervals get longer with decreasing temperatures (fig. 7.2). The carriers trapped in deep localized states in the vicinity of the blinking point leave the traps in non radiative processes. The probability for such processes gets lower with decreasing temperature making the carriers stay longer in the traps and thus causing longer off intervals. Counting the intervals spent in the off and the on state shows that for lower temperatures the probabilities for both longer on and off times increase (fig. 7.3).

Due to time constraints and the difficulties in finding suitable two level blinking points it was not possible to analyze two level blinking points over a broader temperature range or ones that can be described on the basis of the quantum jump theory.

7.4 Multi level blinking points

Videos of a area with several multi level blinking points were taken at different temperatures. With lower temperatures the blinking gets weaker until the blinking

7.4 Multi level blinking points

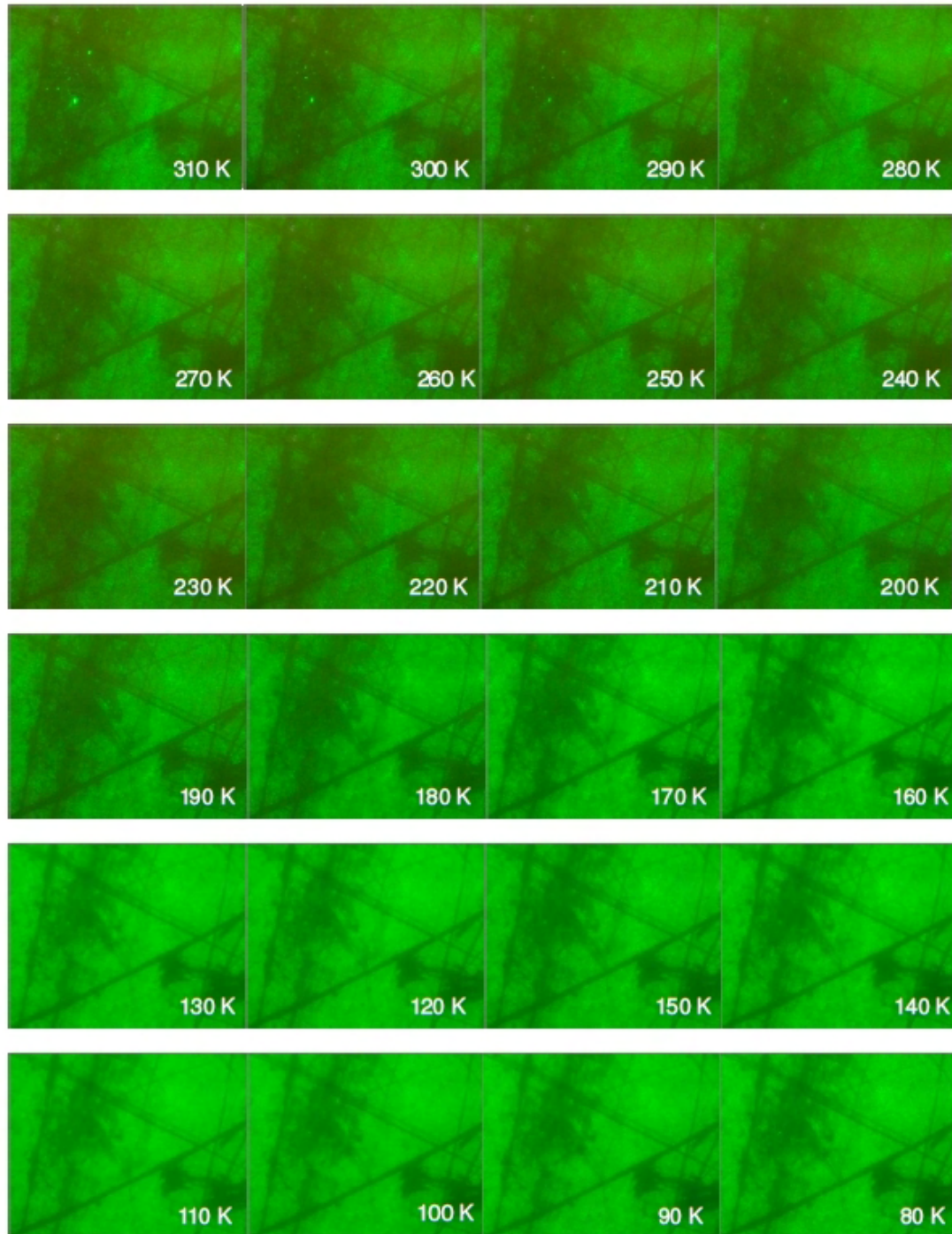


Figure 7.1: The pictures show the photoluminescence of the sample at different temperatures. The left side of the pictures is a area with a small amount of gold enhancing the emission. The right part is covered with a film of gold enhancing the light emission. Many of the bright points in the left half blink. With decreasing temperature the bright points and therewith the blinking points disappear. The overall photoluminescence intensity increases with lower temperatures.

7 Temperature dependence of the blinking

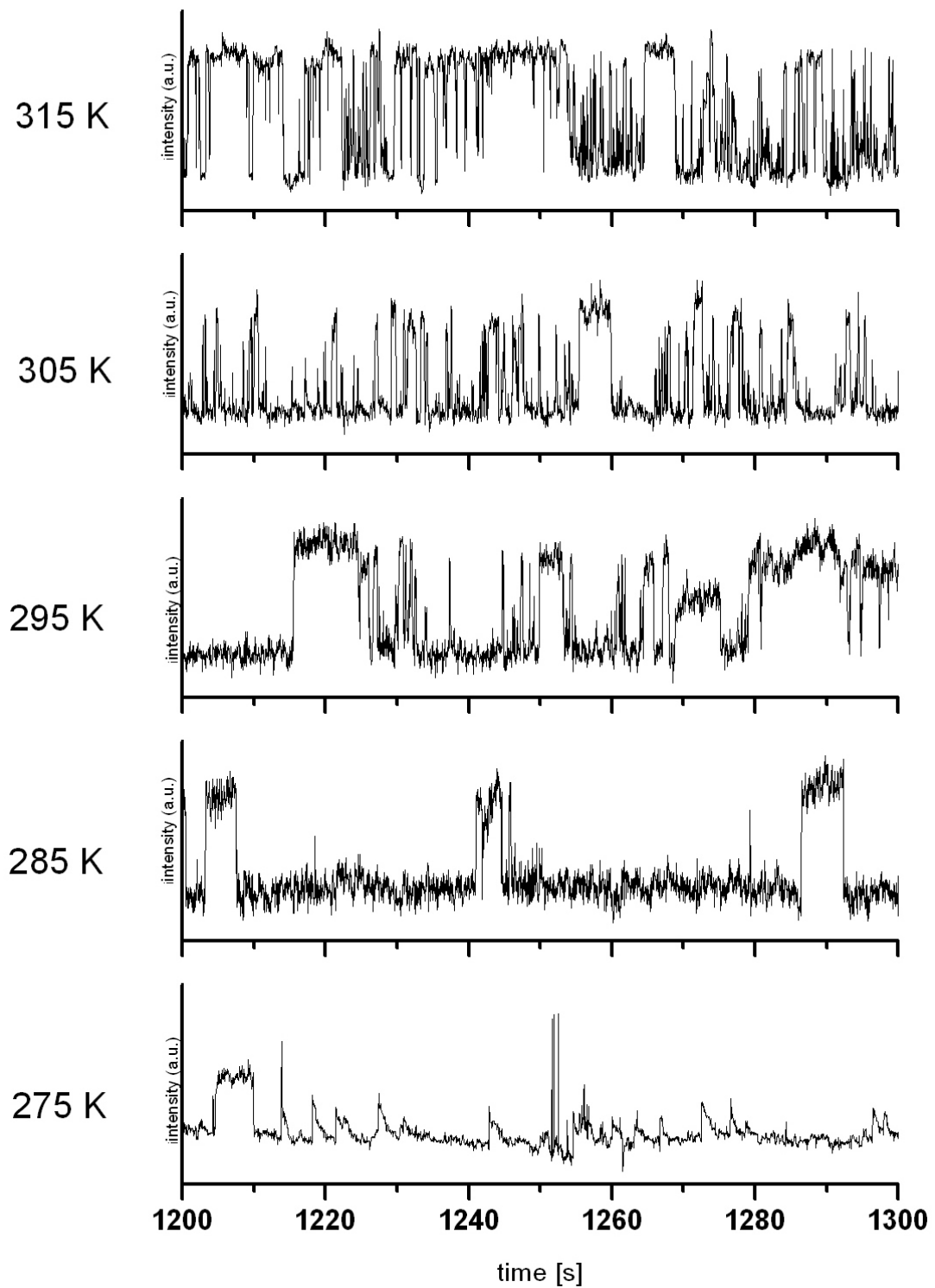


Figure 7.2: 100 s fragments of the photoluminescence intensity time trace of the same two level blinking point show longer off times for lower temperatures.

7.4 Multi level blinking points

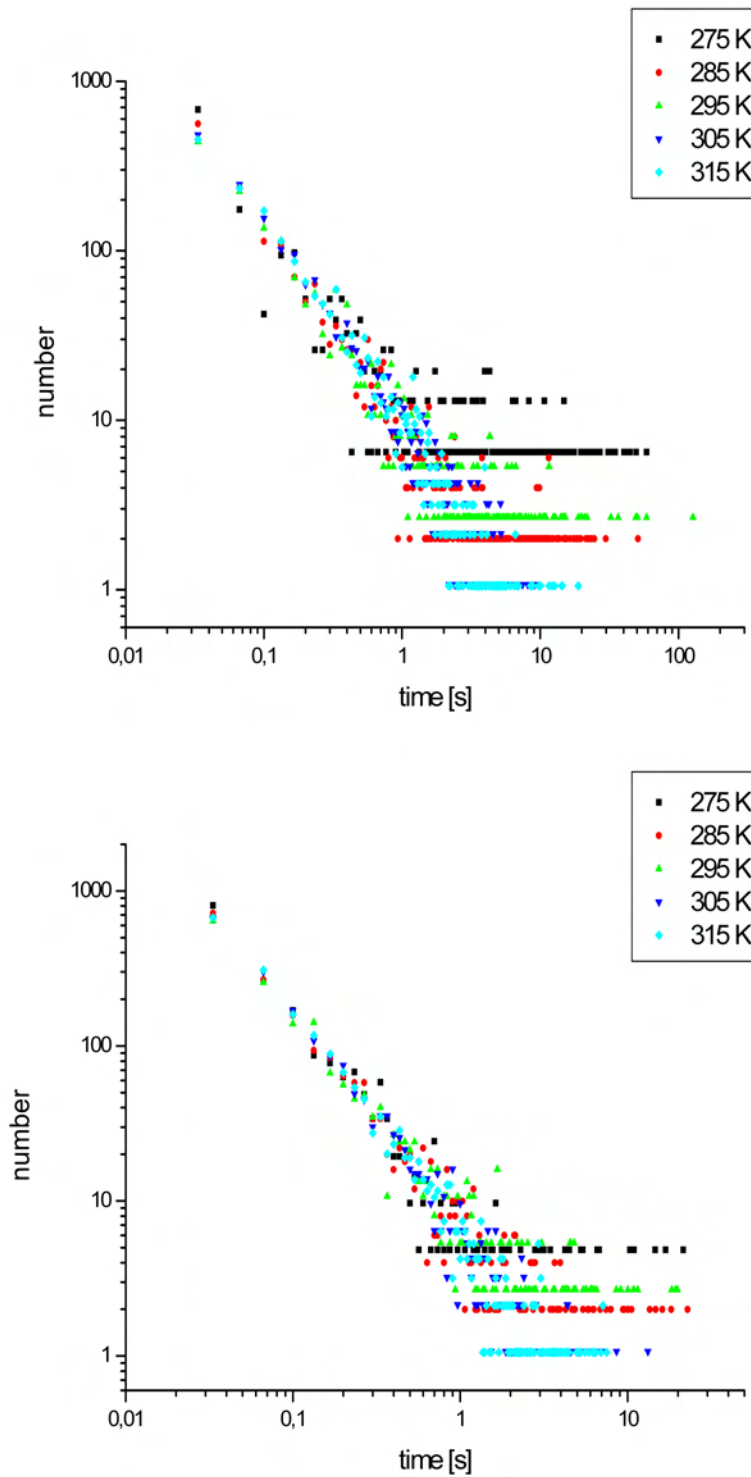


Figure 7.3: Counting the intervals spent in the on (top) and off state (bottom) shows that for lower temperatures the probabilities for both longer on and off times increase

7 Temperature dependence of the blinking

points disappear in the background. This is illustrated by fig. 7.4 and fig. 7.5 that show maps of the standard deviation of the photoluminescence intensity of a area with several multi level blinking points at different temperatures.

The time intensity profiles of one single multi level blinking point at different temperatures are shown in fig. 7.6. At high temperatures the point switches both between distant and close levels. With lower temperatures the average intensity decreases and the point just switches between near intensity levels and not between distant ones anymore. At very low temperatures the blinking points disappears in the background and its noise. A comparison of the intensity histograms of this point at different temperatures confirms these observations (fig. 7.7).

In the case of multi level blinking points the intense light emitting centres couple to several deep traps and all the local electric fields of the traps impact on the blinking point. Traps of different depth i.e. different activation energies for the trapped carriers have different probability distributions for off times. With decreasing temperature the probability for a long off time caused by a carrier in a trap with high activation energy is much higher than for one with smaller activation energy. This means that at low temperatures carriers can rather escape from shallow than from deeper traps. The carriers in deeper traps remain there and thus reduce the average intensity and the blinking only occurs between close intensity levels.

7.4 Multi level blinking points

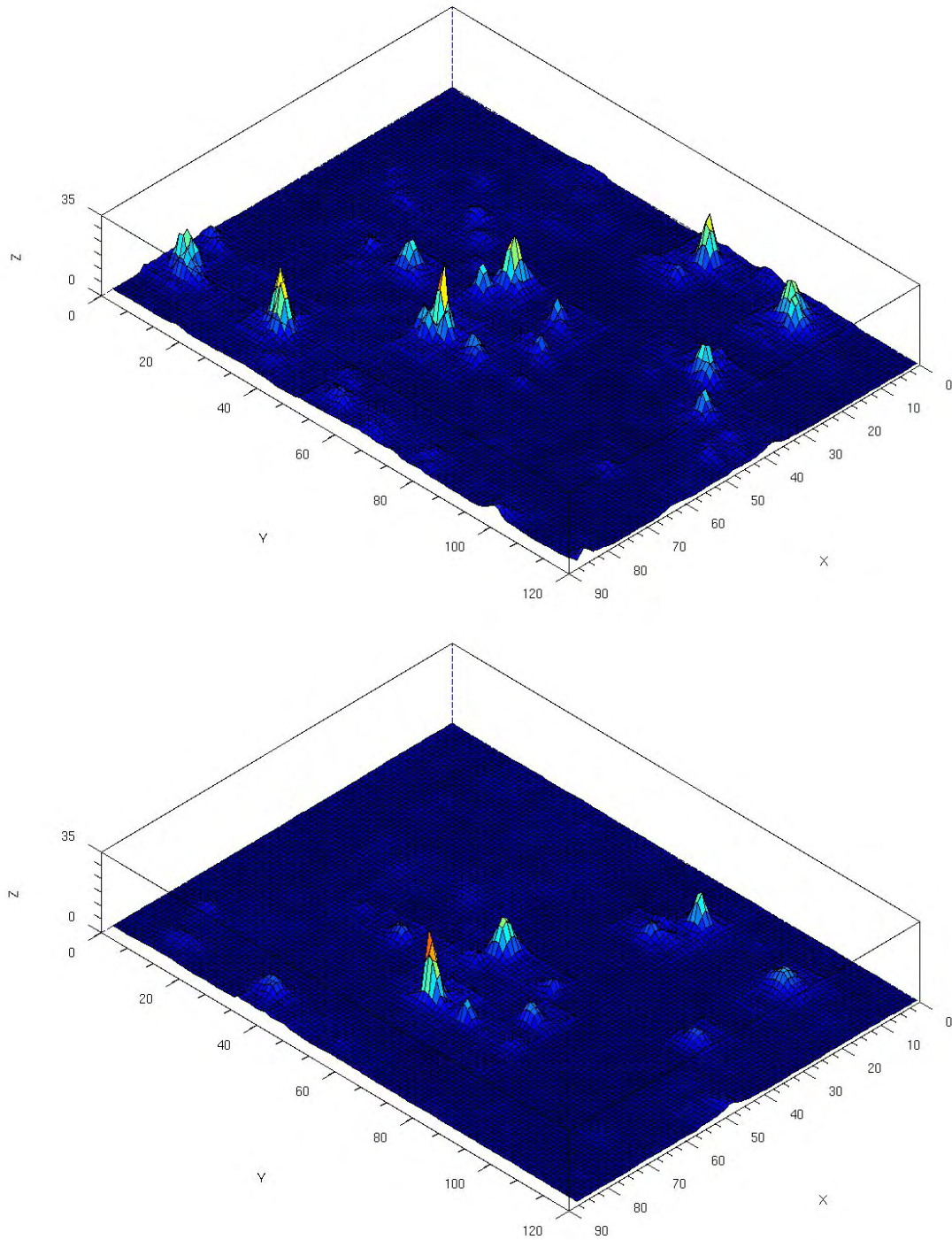


Figure 7.4: The standard deviation of the photoluminescent intensity calculated and mapped for each pixel of a movie file at different temperatures of 310 K (top) and 300 K (bottom). The standard deviation is plotted in z-direction, x and y specify the pixel coordinates. Red points show areas of high standard deviation (blinking points) blue areas correspond to low standard deviation.

7 Temperature dependence of the blinking

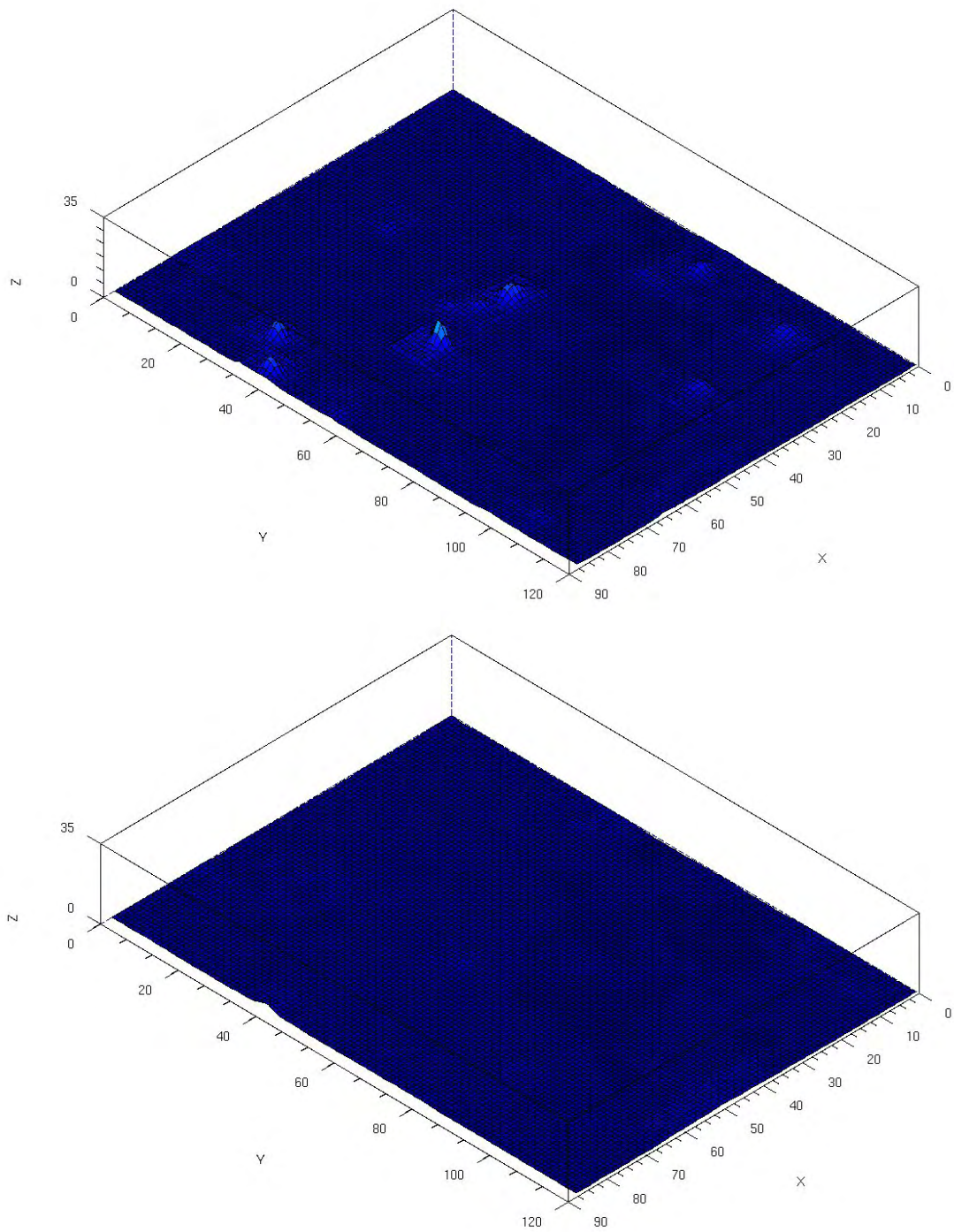


Figure 7.5: The standard deviation of the photoluminescent intensity calculated and mapped for each pixel of a movie file at different temperatures of 280 K (top) and 240 K (bottom). The standard deviation is plotted in z-direction, x and y specify the pixel coordinates. Red points show areas of high standard deviation (blinking points) blue areas correspond to low standard deviation.

7.4 Multi level blinking points

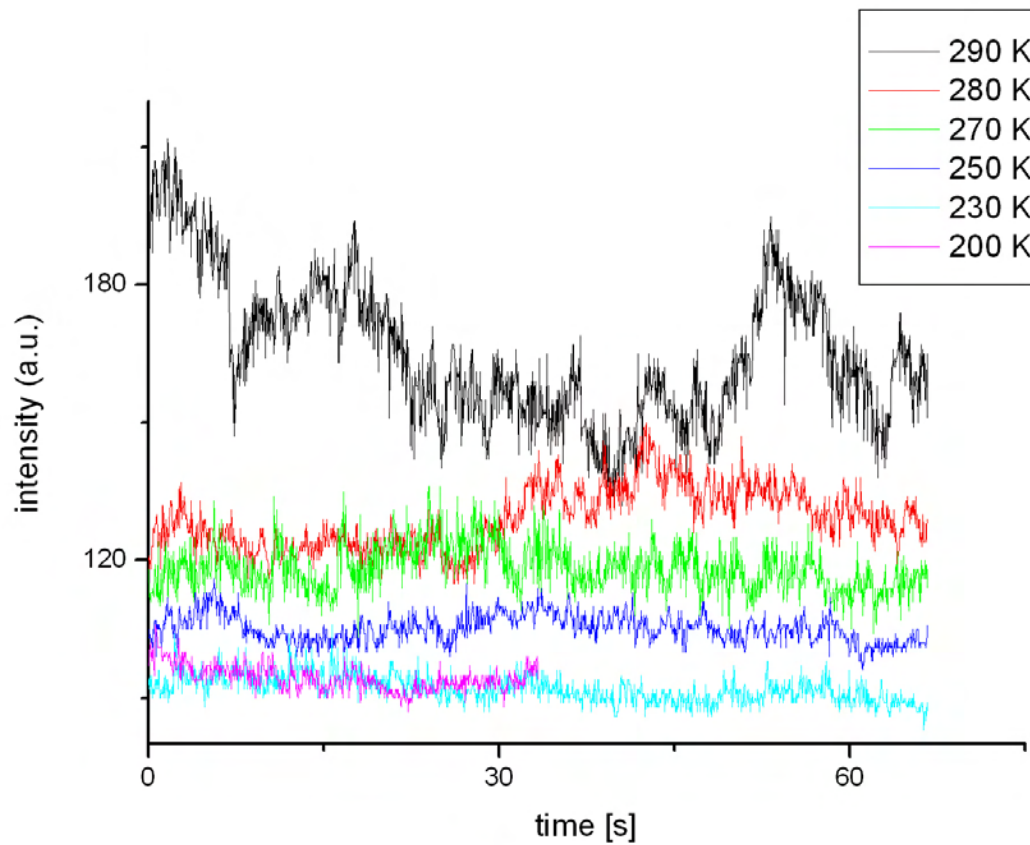


Figure 7.6: The time intensity profiles of the same multi level blinking point at different temperatures. At higher temperatures the average intensity is higher and the point switches between more distant intensity levels than at lower temperatures.

7 Temperature dependence of the blinking

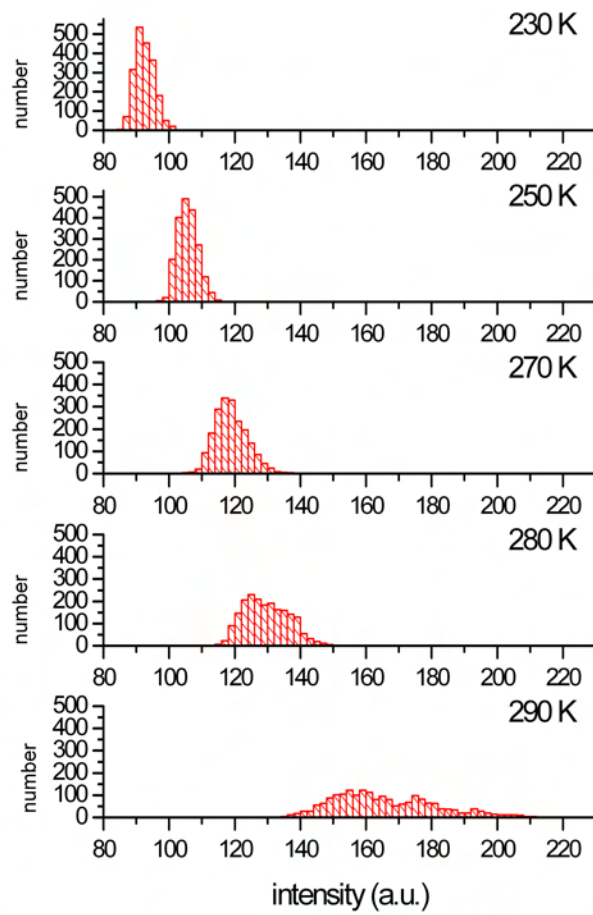


Figure 7.7: The intensity histograms of the same blinking point at different temperatures. With rising temperature the distribution gets brought and the average intensity higher.